Bioactive Materials 21 (2023) 403–421

Contents lists available at ScienceDirect

Bioactive Materials

journal homepage: www.keaipublishing.com/en/journals/bioactive-materials

Promoting lacunar bone regeneration with an injectable hydrogel adaptive to the microenvironment

Ao Zheng [1], Xiao Wang [1], Xianzhen Xin, Lingjie Peng, Tingshu Su, Lingyan Cao [**], Xinquan Jiang [*]

Department of Prosthodontics, Shanghai Ninth People's Hospital, Shanghai Jiao Tong University School of Medicine, College of Stomatology, Shanghai Jiao Tong University, National Center for Stomatology, National Clinical Research Center for Oral Diseases, Shanghai Key Laboratory of Stomatology, Shanghai Engineering Research Center of Advanced Dental Technology and Materials, 639 Zhizaoju Road, Shanghai, 200011, China

ARTICLE INFO

Keywords:
Injectable hydrogel
Oral and maxillofacial
Silk fibroin
Lacunar bone deficiency
Bone regeneration

ABSTRACT

Injectable hydrogel is suitable for the repair of lacunar bone deficiency. This study fabricated an injectable, self-adaptive silk fibroin/mesoporous bioglass/sodium alginate (SMS) composite hydrogel system. With controllable and adjustable physical and chemical properties, the SMS hydrogel could be easily optimized adaptively to different clinical applications. The SMS hydrogel effectively showed great injectability and shapeability, allowing defect filling with no gap. Moreover, the SMS hydrogel displayed self-adaptability in mechanical reinforcement and degradation, responsive to the concentration of Ca^{2+} and inflammatory-like pH value in the microenvironment of bone deficiency, respectively. *In vitro* biological studies indicated that SMS hydrogel could promote osteogenic differentiation of bone marrow mesenchymal stem cells by activation of the MAPK signaling pathway. The SMS hydrogel also could improve migration and tube formation of human umbilical vein endothelial cells. Investigations of the crosstalk between osteoblasts and macrophages confirmed that SMS hydrogel could regulate macrophage polarization from M1 to M2, which could create a specific favorable environment to induce new bone formation and angiogenesis. Meanwhile, SMS hydrogel was proved to be antibacterial, especially for gram-negative bacteria. Furthermore, *in vivo* study indicated that SMS could be easily applied for maxillary sinus elevation, inducing sufficient new bone formation. Thus, it is convincing that SMS hydrogel could be potent in a simple, minimally invasive and efficient treatment for the repair of lacunar bone deficiency.

1. Introduction

The oral and maxillofacial region with specific anatomical structures bears multiple critical physiological functions such as chewing, swallowing, speech et al. Bone deficiency in this region will affect the appearance and lead to oral dysfunction, interfering with the quality of life and psychological health of patients [1]. Bone defects or deficiency caused by tumors, trauma, or physiological factors in the oral and maxillofacial region, often present irregular and lacunar characteristics. For example, the maxillary sinus is a typical irregular lacunar structure in the oral and maxillofacial region. Maxillary sinus floor lifting is often required clinically to solve bone deficiency during dental implantation. Although bone powder and other granular materials are commonly employed in oral clinic for repairing bone deficiency, many problems still exist, such as complicated operations, shape matching difficulties, and enormous trauma caused. Therefore, developing injectable regenerative repair materials suitable for minimally invasive surgery has become a hot spot in the oral clinic.

Injectable hydrogel with similar porous structures to the extracellular matrix (ECM) is recognized to be superior in repairing lacunar bone deficiency. The internal-connected pores are mainly filled with water, which is beneficial for exchanging nutrients and transportation of drugs, so as to be conducive to cell survival and proliferation [2]. Silk fibroin (SF), known for its injectable property and excellent biocompatibility, has been widely adopted in tissue engineering [3–6]. However, according to our previous study, the preparation of SF hydrogel required

Peer review under responsibility of KeAi Communications Co., Ltd.
* Corresponding author.
** Corresponding author.
E-mail addresses: cly_linya@163.com (L. Cao), xinquanjiang@aliyun.com (X. Jiang).
[1] Ao Zheng and Xiao Wang contributed equally to this work.

https://doi.org/10.1016/j.bioactmat.2022.08.031
Received 11 February 2022; Received in revised form 7 August 2022; Accepted 14 August 2022

additional ultrasound treatment, which was not controllable and convenient in clinical applications [7]. In addition, the pure SF hydrogel has the limitations of relatively dense internal pores and poor degradation, which could not meet the needs of tissue regeneration. Therefore, it is necessary to integrate it with other ingredients to fulfill the clinical requirements [8]. Sodium alginate (SA), a natural polysaccharide with good biocompatibility, has been reported as a regulator in SF hydrogel to improve its physical and chemical properties, such as porosity [9]. SA can immediately crosslink once encountered upon Ca^{2+} [10]. $CaCl_2$ is commonly adopted as a crosslinking agent in traditional alginate-based gel systems. However, it is difficult to control the gelation rate and easy to result in gel inhomogeneity [11]. Therefore, regulation of the Ca^{2+} distribution in SA solution before gelation is a pending-solved problem in the application of SA hydrogels.

Bioactive mesoporous glass (MBG) is a kind of inorganic non-metallic material with good biological activity and adjustable function [12], with advantages of large specific surface area, uniform pore size, and large pore volume. MBG also has good osteogenic activity and can be employed for bone repair [13–15]. Significantly, MBG can slowly release Ca^{2+}, Si^{2+}, and doped ions such as Zn^{2+} and Sr^{2+} [16,17], which possibly could be utilized to induce the gelation of SA hydrogel. Moreover, it was reported that Ca^{2+} could accelerate the folding process of the hydrophilic chain in the SF molecule, thus speeding up the formation of SF hydrogel [18]. We assumed that if MBG could be evenly distributed in SF/SA mixture solution in advance, followed by the addition of natural weak acid molecules such as vitamin C (ascorbic acid, VC) that could stimulate in situ dissolution of MBG and adjust the Ca^{2+} release, the uniform and controllable crosslinking of SF/SA composite hydrogel would be achieved. Meanwhile, as the local microenvironment of MBG degradation is alkaline, the introduced weak acid could also conducive to adjusting the pH value of the microenvironment. Furthermore, the degradation of MBG could form a porous structure inside the hydrogel. Therefore, MBG was chosen as the crosslinking and pore-forming agent to develop an interpenetrating network hydrogel (SF/MBG/SA, SMS) based on SF and SA hybrid system.

The SMS hydrogel constructed in this study was hypothesized to have adaptively enhanced mechanical performances and environment-responsive degradation properties. Since there possesses a particular concentration of Ca^{2+} in the bone defect area [19], the SMS hydrogel is assumed to have enhancement potentiality in strength and stability derived from SA crosslinking by the Ca^{2+} physiological environment. When the inflammatory reaction/infection occurs in the implanted area, the surrounding environment becomes weakly acidic [20–23]. It would most likely stimulate the Ca^{2+} release from the remaining MBG in SMS hydrogel to trigger the continuous gelation. In this way, the SMS hydrogel could neutralize the acidity of the microenvironment in situ, which might inhibit the local bacterial growth. Moreover, cells would easily grow into the hydrogel to guarantee rapid tissue regeneration, as the pore size of the hydrogel increases with the degradation of MBG. Thus, MBG was selected as a Ca^{2+} source to prepare the injectable composite SMS hydrogel, which provided a practical approach to improve the homogeneity of gelation and met the requirements of shape matching in the repair of lacunar bone deficiency.

Based on the optimization and construction of self-adaptive SMS hydrogel, we further employed the effects of hydrogel on cell viability and osteogenic/vascular differentiation of bone marrow mesenchymal stem cells (BMSCs). A rabbit model of maxillary sinus elevation was adopted to elaborate on the effect of biological hydrogel on repairing lacunar bone deficiency. The in-situ forming SMS hydrogel might perfectly fill the defect area at the initial implantation stage, providing an extracellular matrix for cell migration and proliferation. A specific supporting force is gathered in the defect area through the mechanical self-enhancement of hydrogels. In case of infection, it could also degrade responsively in the acidic microenvironment to inhibit infection progress. During the degradation process, the release of Ca and Si ions from hydrogel promoted the osteogenesis and angiogenesis of cells so that they could repair lacunar bone deficiency *in vivo* (Fig. 1). This strategy is expected to provide a feasible, straightforward, minimally invasive treatment for lacunar bone deficiency.

2. Results and discussion

2.1. Preparation and optimization of SMS composite hydrogel system

In this study, an injectable in-situ forming SMS composite hydrogel with controllable physicochemical properties was prepared successfully. The prepared MBG was uniform with typical ordered mesoporous structures (Fig. S1). By changing the content of MBG and VC in SMS hydrogel, the gelation time (Fig. S2. A) of hydrogels and surrounding pH (Fig. S2. B) could be controlled to meet different clinical applications. As the MBG contained in the gel reacted with VC, the shape of the gel could be easily changed with the content of MBG and VC (Fig. 2. A). When VC content was 1.5% (w/v) and the MBG content was 2% (w/v), the surrounding pH of the hydrogel was about 7.6, which was slightly alkaline. With the increase of VC content, the compressive strength of the composite hydrogel first increased and then decreased (Fig. S2. C), which reached the peak value in the hybrid system with an MBG content of 2%. When the VC concentration was increased from 0.5% to 2.0%, the compressive strength of SMS hydrogels increased. It is because the low VC concentration induced a slow degradation of MBG as well as a gradually increased release of Ca ions. As a result, the crosslinking and the compressive strength of SMS hydrogels were strengthened. When the VC concentration exceeded 2.0%, the reaction rate of MBG with VC significantly accelerated, thereby the release of Ca ion increased suddenly, which made the crosslinking of SA in the composite uneven and uncontrollable. Thus, the homogeneity of the structure was destroyed, resulting in the strength decrease of the SMS hydrogel.

In the SMS system, MBG was employed as the crosslinking ion source of the hydrogel system. By introducing VC, the rate of Ca^{2+} released from MBG was organized to control the crosslinking speed. Meanwhile, the released Ca^{2+} could promote the β-sheet transformation of silk fibroin to enhance the stability of the hydrogel network. By adjusting the content of MBG and VC in the system, the gelation time, compressive strength and surrounding pH value of SMS composite hydrogels could be integrated to fulfill the demands of diverse clinical applications. Considering our purpose, the pH, gelation time and strength of the composite hydrogels, we have chosen SMS composite hydrogels with VC content of 1.5% and MBG content of 2% for the next spotlight.

2.2. Characterization of SMS hydrogel

Bone defect filling materials usually need good mechanical properties to adapt to the compression of surrounding tissues [24,25]. The SMS hydrogel exhibited good injectable properties, forming homogeneous hydrogels in situ. The pre-gel solution could be easily extruded from a syringe with needle No. 23 to create different shapes (Fig. 2. B). The excellent injectable properties of the SMS hydrogels enable the material to be filled through tiny wounds and reduce surgical trauma. Meanwhile, it had good shapeability so that hydrogels could be filled in the irregularly shaped lacuna and seamlessly connect with surrounding tissues with uniform structures (Fig. 2. C).

Fig. 3. A presented the SEM images of SMS hydrogel. The cross-sections of SMS were sponge-like with perforated internal holes and MBG was evenly distributed. The distribution of MBG on the pore wall could increase the roughness of the pore wall, serving as the mineralization center to promote cell mineralization [26]. The internal pore size of SMS hydrogel was between 150–200 μm, which is suitable for wrapping cells, cell growth and exchange of nutrients, larger than the internal pore diameter of SF hydrogel (50–100 μm) (Fig. S3) [27]. The introduction of MBG and SA has increased the pore size of SF hydrogel. ICP results demonstrated that Ca and Si ions were released rapidly in the first 2 weeks in the SMS hydrogel group, while nearly no ions were

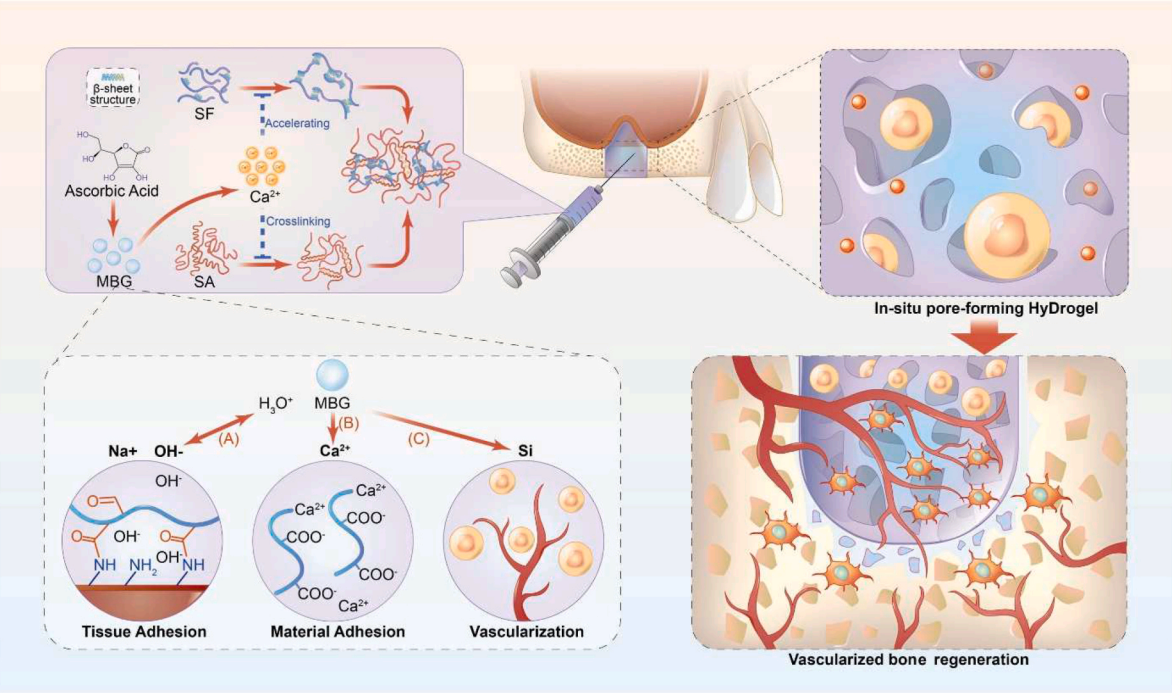

Fig. 1. Schematic illustration of the injectable SMS hydrogel.

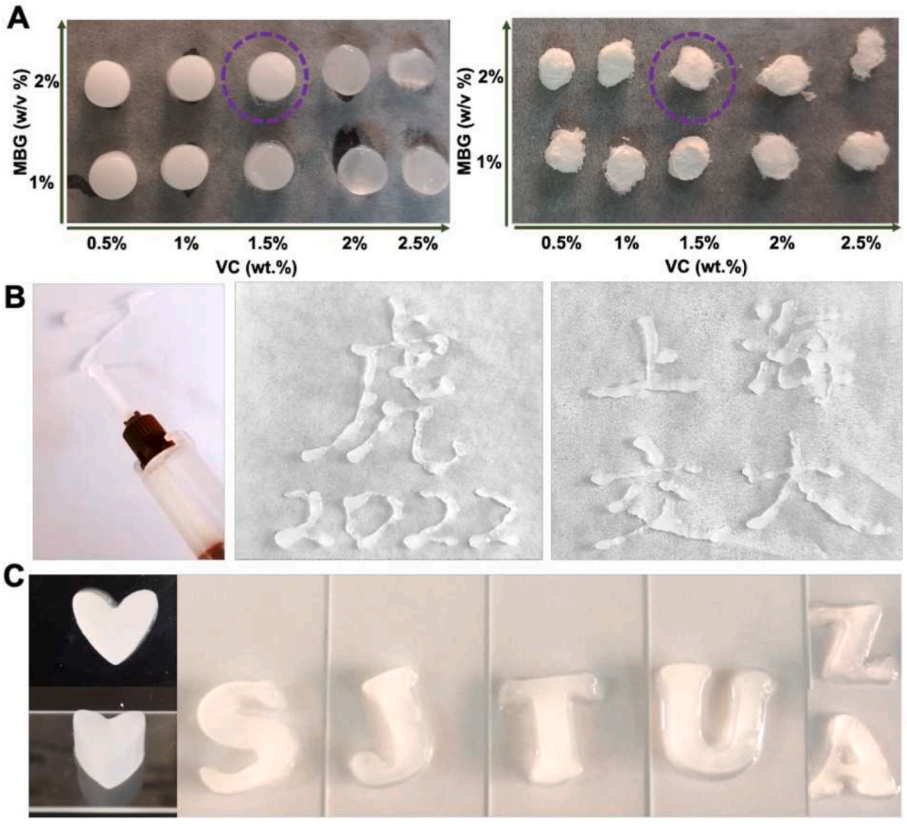

Fig. 2. Preparation and characterization of injectable SMS hydrogel system. A) Digital photograph of the morphology of wet and freeze-dried composite SMS hydrogels with different amounts of VC and MBG. The composite hydrogel with 2% MBG and 1.5% VC (purple circle: SMS hydrogel) was chosen for further study. B) Digital photographs of the SMS hydrogel injected via a fine needle. C) Evaluation of the shapeability of SMS hydrogel in different modulus.

released from SF hydrogel. This result indicated that MBG in the SMS group could continuously release bioactive ions (Fig. S4). As reported, Ca and Si ions could induce osteogenic differentiation and mineralization [28,29].

As a potential practical application in clinic, SMS Hydrogel could meet the need for rapid in situ gelation and high strength. The

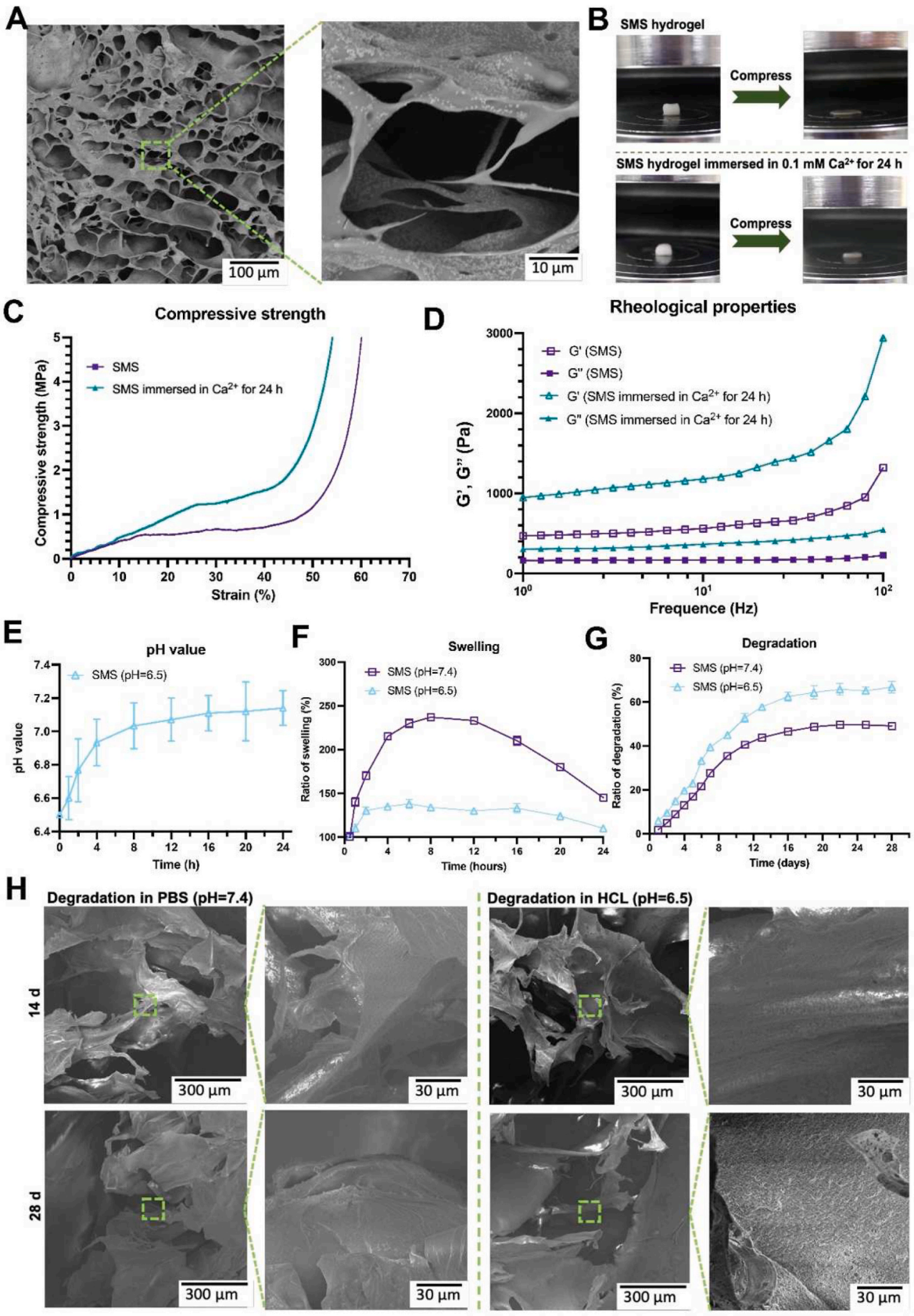

Fig. 3. A) SEM images of SMS hydrogel. B) Compression testing, C) Strain-Stress curve and D) Rheological behavior of SMS hydrogel and SMS hydrogel immersed in 0.1 mM Ca^{2+} for 24 h. E) pH changes of SMS hydrogel soaked in HCl solution (pH = 6.5). F) *In vitro* swelling and G) degradation of SMS hydrogel in PBS (pH = 7.4) and HCl solution (pH = 6.5). H) SEM images of SMS hydrogel residuals after immersion in PBS (pH = 7.4) and HCl solution (pH = 6.5) for 14 days and 28 days, respectively.

compressive test results show that the compressive strength of SMS hydrogel is ~0.5 MPa (Fig. S5), while the compressive strength of the composite hydrogel significantly increased after being immersed in Ca^{2+} for 24 h. The SMS hydrogel immersed in Ca^{2+} for 24 h had a higher modulus of elasticity and compression deformation (Fig. 3. B and C). The G′ of SMS hydrogel in the frequency range is higher than G″, indicating that the SMS hydrogel was viscoelastic and the storage modulus of SMS hydrogel immersed in Ca^{2+} for 24 h was elevated significantly (Fig. 3. D). As the concentration of Ca^{2+} in the human extracellular fluid is about 0.1–3.0 mM [30], once SMS hydrogel is implanted *in vivo*, the mechanical strength of SMS hydrogel will be enhanced adaptively and continuously. Meanwhile, mechanical properties could support the bone

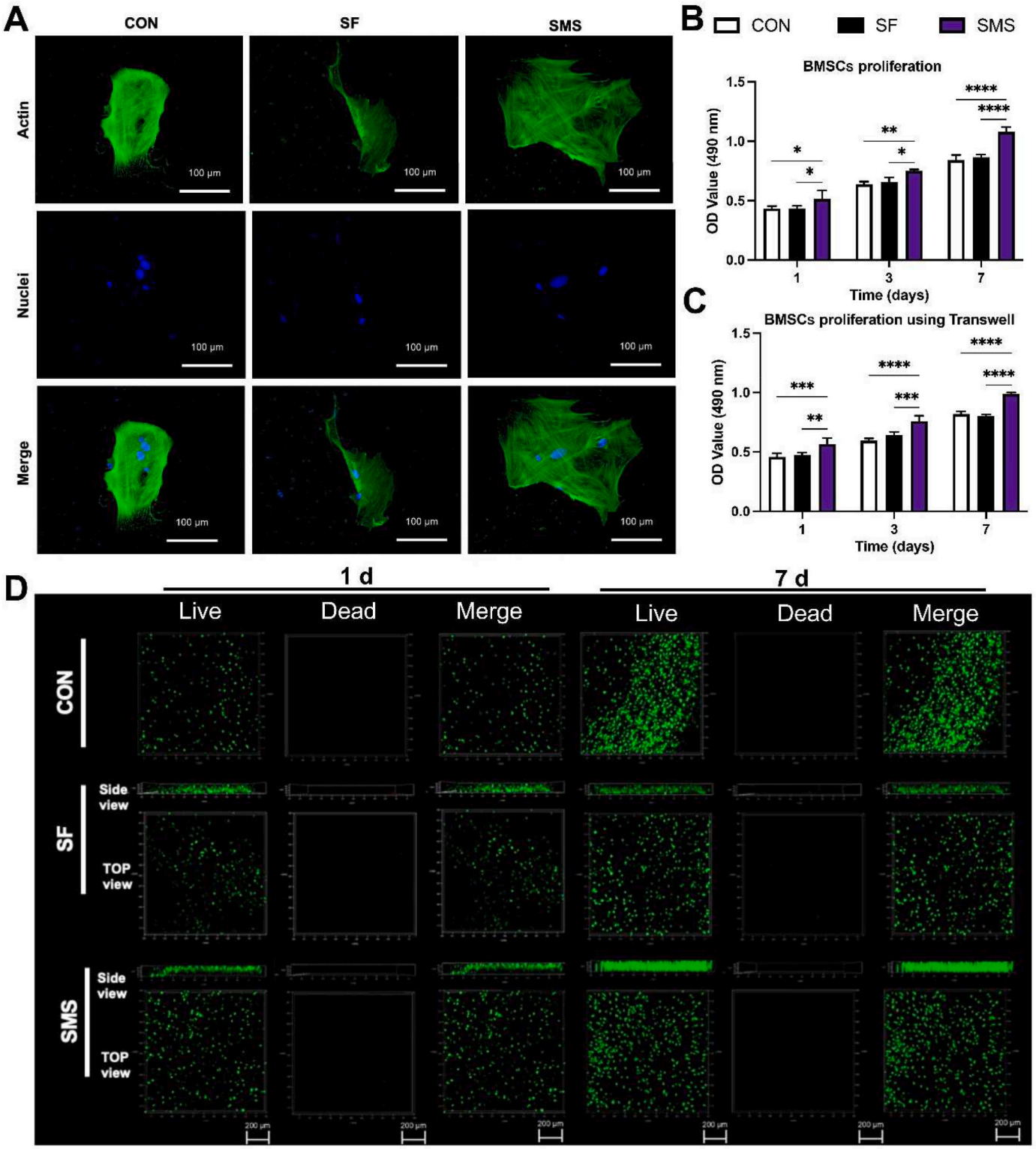

Fig. 4. Cell adhesion and viability assay. A) Fluorescence staining of BMSCs cultured on different samples for 12 h. The CCK-8 assay of B) BMSCs seeded on the samples and C) BMSCs cultured with hydrogels using transwell. D) Live/dead staining of BMSCs seeded on different samples. Live cells appeared green, whereas dead cells appeared red. (*$p < 0.05$, **$p < 0.01$, ***$p < 0.005$, ****$p < 0.001$).

defect area and induce the osteogenic differentiation of BMSCs.

We have investigated the effect of hydrogels on the surrounding pH value. It is known that the pH value of an infected or defected site is often 5.0–6.5 [22,31,32]. Hence, HCl solution (pH = 6.5) was selected in this study to mimic the microenvironment with infection or defect, while phosphate buffer saline (PBS, pH = 7.4) was used to simulate the condition in normal tissues. The results of SMS hydrogel immersed in HCl solution (pH = 6.5) showed that the pH value of the solution increased with the degradation of SMS hydrogel. After SMS was immersed in HCl solution for 24 h, the pH value reached 7.4 (Fig. 3. E). After soaking in PBS for 8 h, the swelling ratio of SMS composite hydrogel reached a peak of ~237% (Fig. 3. F). While soaked in HCl solution (pH = 6.5), the swelling ratio of SMS hydrogel reached ~130% and maintained in a relatively stable state after about 2 h. With the proper swelling rate, the shape and mechanical stability of the composite hydrogel could be maintained [33,34]. Thus, with a suitable swelling rate, the SMS could be bonded to the normal tissue around the defect without causing too much pressure. Fig. 3. G showed that SMS composite hydrogel degraded with the extension of immersion time in PBS solution (pH = 7.4) and HCl solution (pH = 6.5). The degradation of SMS composite hydrogel was faster in HCl solution (pH = 6.5) and reached about 50% at 28 days. The SMS composite hydrogel remained intact until 28 days, and the SEM results (Fig. 3. H) showed that the residuals got more porous than before. These results indicate that when the infection occurs in the defect, the SMS hydrogel was degraded faster to neutralize the microenvironment to relieve the inflammation, and thus induced the cells to grow in and accelerate the tissue regeneration simultaneously.

2.3. Effect of SMS composite hydrogel on BMSCs activity and proliferation ability

Early cell adhesion is essential for subsequent cell differentiation, directly affecting subsequent biological behavior [35]. After BMSCs were cultured on different hydrogels for 12 h, the cytoskeleton was stained and imaged. BMSCs adhered to the surface of the SMS hydrogel and spread well with polygonal structures (Fig. 4. A).

Cytotoxicity of SMS composite hydrogel was detected by the CCK-8 test (Fig. 4. B). From the results, it could be judged that the cell proliferation in the SMS composite hydrogel was faster than that in group SF and CON at each time point, while there was no significant difference between the SF group and CON group, and the cells in the three groups significantly increased as time went on. Transwell co-culture has been widely employed in detecting material biology to simplify the experimental operation in cell culture [36]. Cell proliferation of BMSCs co-cultured with hydrogel using transwell was also detected. It could be estimated from Fig. 4. C that the number of live cells in group SMS was significantly higher than in group CON at every time point, identical to those in cells seeded on the gel. By comparison of the cell viability of BMSCs seeded on SMS hydrogel to the co-culture in transwell, we could speculate SMS hydrogel surface is friendly for BMSCs to grow on. Studies have shown that Ca^{2+} ions in the solution could promote the proliferation of BMSCs [37]. Thus, cell proliferation might be correlated with the ions released from the SMS composite hydrogel in the solution.

Improving the survival rate of stem cells after implantation is closely related to tissue repair [38]. In the live/dead experiment, the green color represents living cells while the red represents dead cells in Fig. 4. D, we could estimate more green fluorescence spots, and almost no red fluorescence spots appear in the composite hydrogel group and the SF hydrogel group. After 7 days of culture *in vitro*, a prominent proliferation of live BMSCs inside the SMS hydrogel could be found. The experimental results showed that SMS composite hydrogel had good biocompatibility and could effectively promote the adhesion and proliferation of BMSCs. At the same time, the side view of hydrogel also showed that BMSCs seeded on the surface could grow into the SMS hydrogel and proliferate, which was beneficial for cell and tissue ingrowth after implantation *in vivo*.

2.4. Effect of SMS hydrogel on osteogenesis in vitro

As shown in Fig. 5. A, the ALP staining of SMS composite hydrogel was more profound than that of the SF group and the negative control group, which indicated the most vital expression of ALP among the three groups. As shown in Fig. 5. B, the SMS composite hydrogel group showed calcium deposition after 21 days of osteogenic induction, while the SF hydrogel group did not show this result. After induction prolonged to 28 days, the SMS composite hydrogel group had a much darker and more extensive coverage area compared with other groups, indicating SMS composite hydrogel could promote BMSCs to undergo osteogenic differentiation faster and better, as well as participate in the mineralization process earlier possibly. The results of ALP and ARS semi-quantitative detection were consistent with the staining results (Fig. 5. C and D). Fig. 5. E showed the fluorescence staining results of ALP protein after 7 days of co-culture. The ALP expressed by BMSCs in the SMS group was the most and the brightest, consistent with the above ALP activity detection results. These results indicate that SMS hydrogel could promote the ALP activity and osteogenic differentiation of BMSCs.

In order to remove the effect of initial cell proliferation, the osteogenic ability of each group was quantitatively analyzed. Real-time quantitative reverse transcriptase polymerase chain reaction (qRT-PCR) analysis was employed to study the osteogenesis-related gene expressions of BMSCs co-cultured with hydrogel. After co-cultured with SF and SMS hydrogels for 7 and 14 days, the RUNX2, ALP, Col-1, OPN and OCN expressions of BMSCs in the SMS composite hydrogel group were significantly higher than that in the SF and CON group ($p < 0.05$) (Fig. 5. F–K). Meanwhile, after culture with hydrogels for 3 days, BMSCs had already displayed the up-regulated relative gene expression of RUNX2 and ALP in the SMS group. This result indicated that SMS hydrogel could promote the early-stage osteogenic differentiation of BMSCs (Fig. S6). ALP is an important osteoblast activity marker in the process of early osteoblast differentiation, whose activity increases with the increase of bone activity [39]. RUNX2 is also an important bone transcription factor responsible for osteoblast differentiation, bone formation, and remodeling [40]. Angiogenesis is closely related to bone regeneration. After 7 and 14 days of co-culture, qRT-PCR results showed that the expression of angiogenesis-related gene VEGF of BMSCs in group SMS was highest (Fig. 5. J). We could conclude that the SMS hydrogel was capable of promoting osteogenic differentiation of BMSCs through up-regulating their expressions of osteogenesis-related genes.

2.5. Relationship between immunity and osteogenesis in vitro

As shown in Fig. 6. A and B, RAW 264.7 cells could grow on the surface of hydrogel, while the proliferation trend of cells is consistent with that of BMSCs. Our results (Fig. 6. C and D) showed that the pro-inflammatory gene expressions of IL-β and TNF-α in the SMS group on day 3 were higher than that in the other groups ($p < 0.05$). While on day 7, IL-1β and TNF-α expressions decreased in the SMS hydrogel group. The pro-inflammatory activity of macrophages is mainly caused by TNF-α. This cytokine can actively regulate tissue repair and regeneration in some cases, but the excess will destroy the healing process [41]. The expression of TNF-α in the SMS group increased first on day 3 and then decreased on day 7, indicating the formation of a suitable regenerative microenvironment.

From day 3 to day 7, the anti-inflammatory gene expressions of IL-10 and TGF-β in the SMS group continually increased to the highest compared with other groups on day 7 (Fig. 6. E and F). Meanwhile, the anti-inflammatory cytokine IL-10 is also crucial for tissue repair and regeneration, which is involved in transforming M1 macrophages into M2 macrophages [42]. The increased expression of IL-10 in the SMS group indicated that these samples might promote M2 polarization and be conducive to long-term repair.

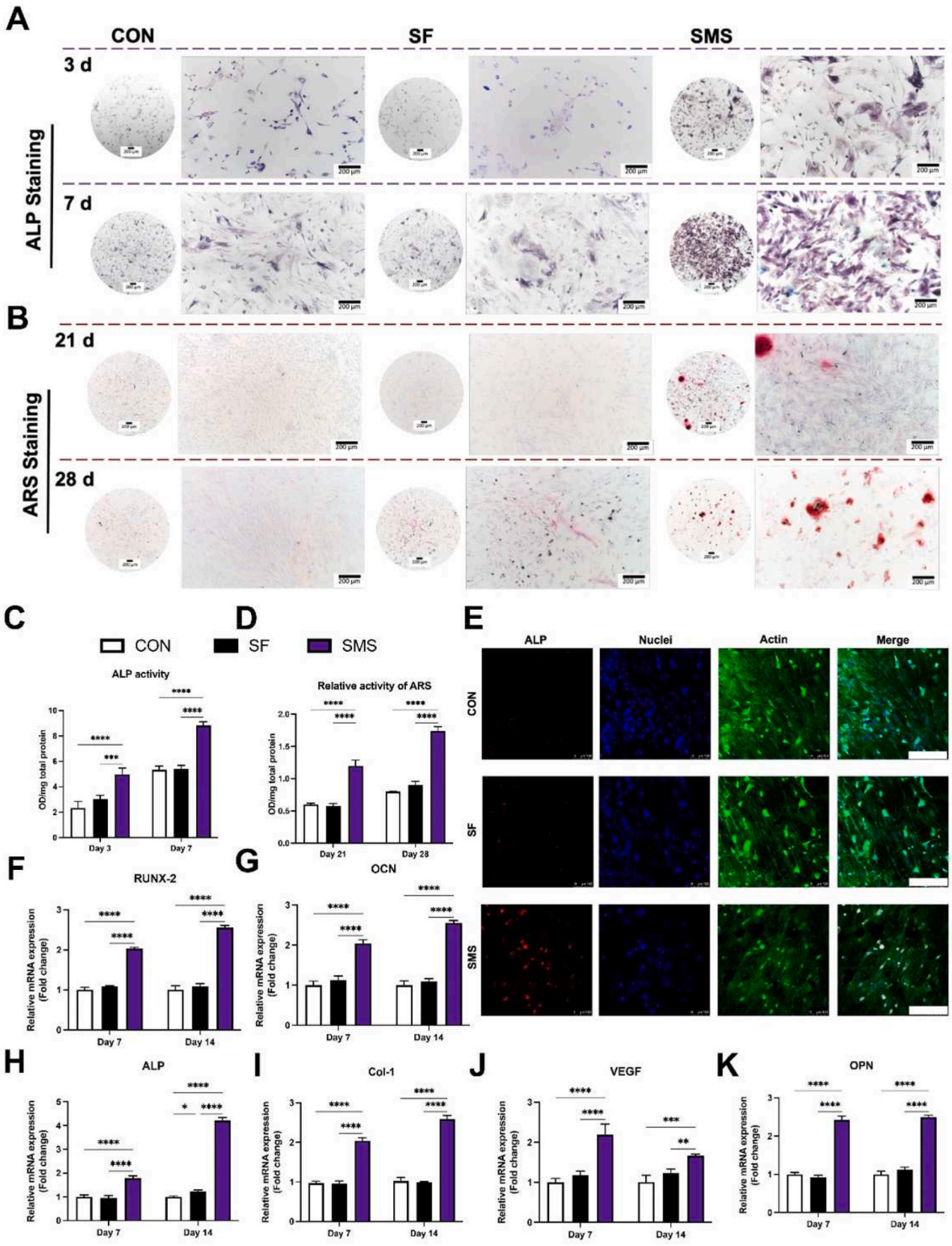

Fig. 5. Osteogenic differentiation assay. A) ALP staining of BMSCs co-cultured with samples for 3 and 7 days. B) ARS staining of BMSCs co-cultured with samples for 21 and 28 days. C) ALP activity of BMSCs co-cultured with samples for 3 and 7 days. D) Relative activity of ARS of BMSCs co-cultured with samples for 21 and 28 days. E) Immunofluorescence staining of ALP expression in BMSCs co-cultured with samples for 7 days. (Scale bar = 200 μm; red: ALP protein; blue: nuclei; green: actin cytoskeleton). Gene expressions of F) RUNX2, G) OCN, H) ALP, I) Col-1, J) VEGF, and K) OPN in BMSCs co-cultured with hydrogels for 7 and 14 days. (White column: Con group; black column: SF hydrogel; purple column: SMS hydrogel; *$p < 0.05$, **$p < 0.01$, ***$p < 0.005$, ****$p < 0.001$).

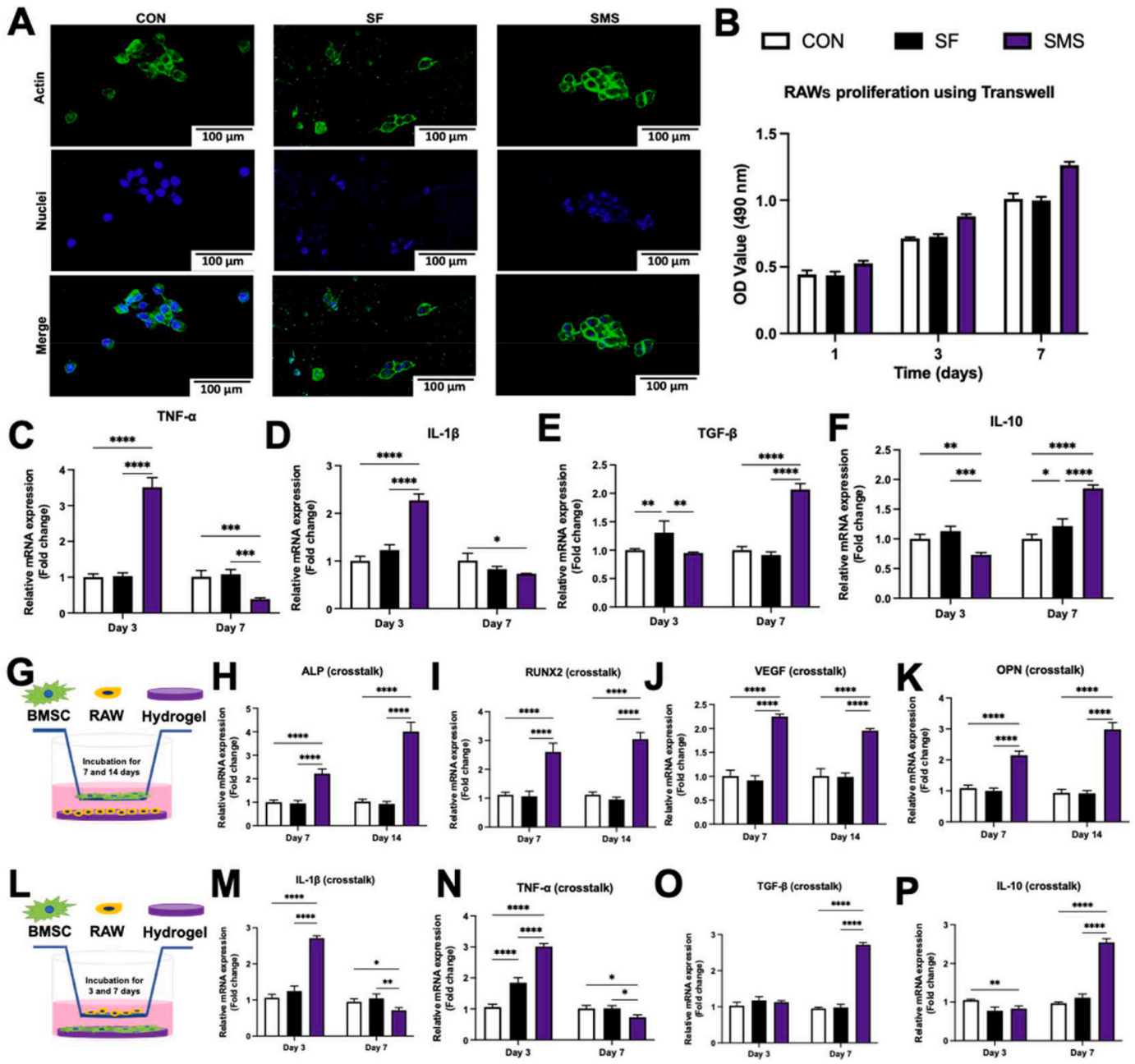

Fig. 6. The crosstalk between BMSCs and RAWs. A) Cell morphology observation. RAW 264.7 cells were cultured on different samples for 24 h. B) The CCK-8 assays of RAW 264.7 cells cultured with hydrogels using a transwell plate. Relative gene expressions of M1 phenotype markers in macrophages: C) TNF-α and D) IL-1β. Relative gene expressions of M2 phenotype markers in macrophages: E) TGF-β and F) IL-10. RAW 264.7 cells were co-cultured with hydrogels for 3 and 7 days. G) Schematic experimental design for investigating the effects of RAWs cultured with SMS hydrogel on the osteogenic differentiation of BMSCs. H–K) Osteogenesis-related gene expressions of ALP, RUNX2, VEGF, OPN, analyzed by qRT-PCR. L) Schematic experimental design for investigating the effects of BMSCs cultured with SMS hydrogel on the polarization of RAWs. M − P) Inflammation-related gene expressions of IL-1β, TNF-α, TGF-β, and IL-10, analyzed by qRT-PCR. (In the histograms C–F, H–K, and M − P, white column: Con group; black column: SF hydrogel; purple column: SMS hydrogel; *$p < 0.05$, **$p < 0.01$, ***$p < 0.005$, ****$p < 0.001$).

Macrophages are the primary infiltrating cells that actively react to the biomaterial implantation and regulate the inflammatory response [43]. The heterogeneity and shapeability of macrophages cultivate them as the main target of immune regulation [44,45]. Although macrophages are essential for regeneration, increased inflammation produced by macrophages can inhibit the regeneration process. Thus, it is important to regulate the response of macrophages [46]. Once the biomaterials are implanted, the surrounding macrophages will be activated to trigger the inflammatory response immediately. Cytokines associated with the M1 phenotype are usually pro-inflammatory factors, such as TNF-α and IL-1β. They mediate the acute response of tissue injury after initial implantation, thus creating an inflammatory microenvironment initiating the bone healing cascade. On the other hand, cytokines related to the M2 phenotype are considered to promote regeneration, such as IL-10 and TGF-β, which help to create an osteogenic microenvironment conducive to tissue repair, including bone formation and remodeling [47]. It is reported that the sustained release of Ca^{2+} from the biomaterials could maintain the long-term induction of M2 macrophage polarization and promote the differentiation of mesenchymal stem cells into osteoblasts during osteogenesis. Furthermore, Ca^{2+} targeted the

Wnt/β-catenin signaling pathway and activated IL-10 (M2 marker genes) transcription through the calcium-sensing receptor (CaSR) in macrophages [48]. Thus, we inferred that SMS hydrogel might transform the immune microenvironment from pro-inflammatory to anti-inflammatory by releasing ions to change the ionic microenvironment, which was beneficial for tissue repair and regeneration.

BMSCs were stimulated by the immune microenvironment induced by RAWs seeded on the SMS hydrogel, whose osteogenic gene expressions were detected by qRT-PCR (Fig. 6. G). The gene expressions of ALP, VEGF, OPN, and RUNX2 in the SMS group were prominent among all the groups and significantly higher than that in the control group ($p < 0.05$) (Fig. 6. H–K). Under co-culture with RAWs seeded on the SMS hydrogel (Fig. 6. I), RUNX2 expression of BMSCs was respectively promoted by ~30% after 7 days and ~20% after 14 days, compared to that under co-culture only with the SMS hydrogel (Fig. 5. F). OPN expression of BMSCs regulated by SMS hydrogel (Fig. 5. K) was also found with an augmentation of ~20% after 14 days of crosstalk with RAWs seeded on the SMS hydrogel (Fig. 6. K). It was shown that MSC survival increased when cells were exposed to M2 macrophages compared with M1 macrophages [49]. Our results showed that the effect of SMS hydrogel to regulate the immune response could further promote the expression of osteogenic genes in BMSCs.

Meanwhile, we also studied whether BMSCs reacted with hydrogels and then regulated macrophage polarization (Fig. 6 L). Compared with other groups, macrophages cultured in BMSCs conditioned medium up-regulated the expression of IL-10 and TGF-β while down-regulated the expression of TNF-α and IL-1β on day 7 (Fig. 6. M – P). The gene expression pattern is consistent with the transformation from the M1 phenotype to the M2 phenotype. Under co-culture with BMSCs seeded on the SMS hydrogel (Fig. 6. O and P), TGF-β and IL-10 expression of RAWs was respectively promoted to ~124% and ~133% after 7 days, compared to that under co-culture only with the SMS hydrogel (Fig. 6. E and F). On this basis, we believed that the SMS hydrogel might further accelerate the M1-to-M2 transition of macrophages by regulating osteogenic gene expressions in BMSCs. We inferred that SMS hydrogel could promote the pro-inflammatory response of macrophages at the early stage of implantation, effectively reduce the pro-inflammatory response, and increase the anti-inflammatory response at the late stage. Regulating the transformation degree of macrophage inflammatory response might be conducive to promoting the immune microenvironment of bone repair and regeneration, and its microenvironment factors could create a specific favorable environment to induce new bone formation and angiogenesis.

2.6. Effect of SMS hydrogel on angiogenesis in vitro

Through the transwell experiment, we verified the migration induced by SMS hydrogel on human umbilical vein endothelial cells (HUVECs). As shown in Fig. 7. A, compared with the control and SF group, more cells were attached to the transwell chamber's lower surface of the polycarbonate membrane in the SMS group. Under the stimulation of SMS hydrogel, more cells migrated from the upper surface to the lower surface compared with the control and SF groups. The number of attached cells in control and SF groups mainly came from the normal migration of cells. The results of the tube forming experiment showed that HUVECs formed well tubular structures after co-cultured with SMS hydrogel under a microscope (Ti–U, Nikon, Japan), indicating that SMS hydrogel had a positive effect on angiogenesis (Fig. 7. B). The quantitative analysis of the tube formation showed that compared with the control and SF groups, the SMS group significantly improved about 4 times in number of circles, number of nodes, and length of branches (Fig. 7. C).

2.7. Antibacterial activity of hydrogels in vitro

In addition to excellent osteogenic induction, the antibacterial ability of materials is crucial for successful bone repair, which prevents postoperative bacterial infection and helps wound healing [50]. According to Fig. 7. D, the ability of SF hydrogel to inhibit bacterial growth was limited, while effective growth inhibition could be clearly observed in the SMS hydrogel group. This result might be attributed to the change in microenvironment pH. The bacterial count method was used to evaluate SMS hydrogel antibacterial activity. The colony count of gram-negative *Escherichia coli* (*E. coli*) or gram-positive *Staphylococcus aureus* (*S. aureus*) in the SMS hydrogel group was smaller than that in the control and SF groups, which was consistent with the result of growth inhibition. SEM results showed no apparent bacterial film-forming phenomenon in the SMS hydrogel group, and only a few bacteria grew (Fig. 7. E). From the different effects on *E. coli* and *S. aureus*, SMS hydrogel seems to have a more potent antibacterial effect on gram-negative bacteria than gram-positive bacteria due to the thicker cell wall of gram-positive bacteria.

2.8. Activation of MAPK signaling pathway in vitro

Osteogenic differentiation is the basis of bone formation and the key step of bone metabolism [51]. A variety of signaling pathways are associated with osteogenic differentiation, including FGF, Wnt/β-Catenin, notch, and MAPK. Multiple signal pathways interact to form a complex regulatory network [51,52]. MAPK pathway is mainly involved in the transduction of extracellular stimuli (growth factors, cytokines, ions et al.) to trigger cell growth, differentiation and apoptosis [52]. Since Erk and JNK pathways are two main MAPK signal transduction pathways [52], we preliminarily studied the phosphorylation of Erk and JNK to verify the activation of MAPK signaling pathway in BMSCs induced by the SMS hydrogel in this study. As shown in Fig. 8. A, the SMS composite hydrogel could facilitate the phosphorylation levels of Erk and JNK. As shown in Fig. 8. B and C, The SMS group significantly enhanced the relative expressions of p-Erk/Erk and p-JNK/JNK, compared with the control (CON) and SF group (****$p < 0.001$). These results indicated that the SMS composite hydrogel could facilitate the phosphorylation of MAPK signaling. Furthermore, by adding inhibitors of Erk1/2 and JNK signaling pathways (PD98059 and SP600125), the phosphorylation levels of Erk1/2 and JNK in BMSCs co-cultured with SMS hydrogel did not increase. The attenuated ALP staining could also be investigated after using the inhibitors (Fig. 8. D-G). Some studies have shown that MAPK signaling pathway can regulate the expression of osteogenic genes through RUNX2-specific serine residue phosphorylation [53]. As mentioned above, the gene expression of RUNX2 in BMSCs co-cultured with SMS hydrogel was significantly higher than that in the CON group at both early (3 days, Fig. S6) and late stages (7 and 14 days, Fig. 5). Meanwhile, some research showed that the released ions such as Ca^{2+} and Si^{2+} could promote osteogenic differentiation through MAPK signaling pathway [54,55]. Therefore, we speculated that SMS hydrogel might regulate osteogenesis in BMSCs through bioactive ions release to activate MAPK signaling pathway.

In addition, MAPK signaling pathway is also involved in immune responses caused by macrophages [51]. Cai et al. [56] reported that the Ti-nanotube (TNT110) could effectively aggravate early inflammatory responses of RAW264.7 cells by up-regulating ITG-mediated MAPK, which further increased the expressions of osteogenesis and chemokine genes. TNT110 could cause the crosstalk between MSCs and RAW264.7 cells, which played a key role in increasing the M1-to-M2 transition of macrophages and promoting early osteogenic induction. In our study, Fig. 6 showed similar results above that SMS hydrogel also caused crosstalk between RAWs and BMSCs, which significantly promoted anti-inflammatory polarization (M2 phenotype) of RAWs and osteogenic differentiation of BMSCs. This regulation was possibly related to the change of the ionic microenvironment between hydrogel and cell by the bioactive ions (Ca^{2+}, Si^{2+}) released from SMS hydrogel [51].

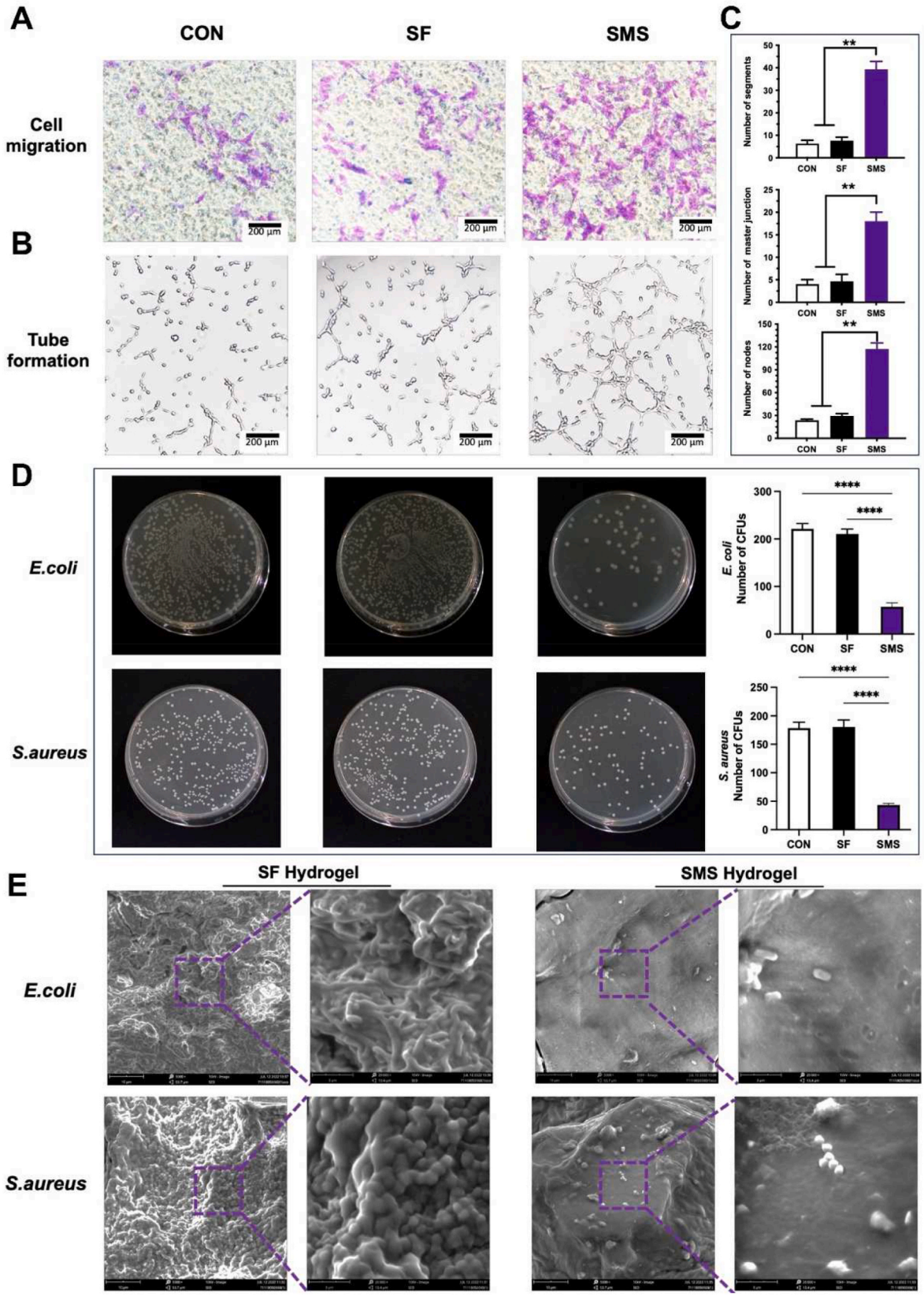

Fig. 7. *In vitro* angiogenesis and antibacterial activity. A) Cell migration assay of HUVECs. B–C) Tube formation of HUVECs cultured on different samples for 24 h and the related quantitative analysis (**$p < 0.01$, ****$p < 0.001$). D) Representative images of colony-forming assays against *E. coli* (upper row) and *S. aureus* (following row). Bacteria were incubated with deionized water (CON), SF hydrogel, and SMS hydrogel. E) SEM observation of biofilm formation on the surface of SF and SMS hydrogels after 10 h of incubation.

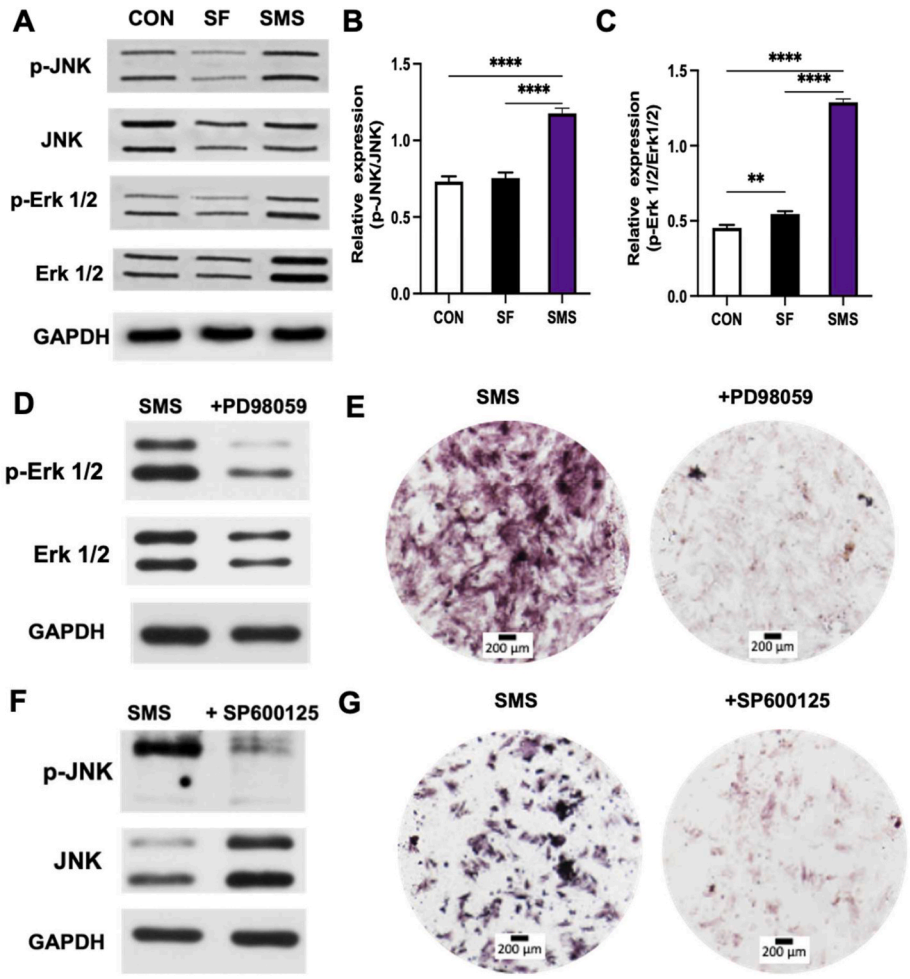

Fig. 8. Investigation of the osteoinductive mechanisms of SMS hydrogel. A-C) Western blot assays show the phosphorylation of MAPK pathway components in BMSCs (****p < 0.001). D) Western blot assays show the inhibitory effects of PD98059, a specific Erk1/2 inhibitor, on activating Erk1/2 (60 min) induced by SMS hydrogel. E) ALP staining of BMSCs treated with or without PD98059. F) Western blot assays show the inhibitory effects of SP600125, a specific JNK inhibitor, on activating JNK (60 min) induced by SMS hydrogel. G) ALP staining of BMSCs treated with or without SP600125.

2.9. The bone regeneration ability of SMS hydrogel in vivo

The rabbit maxillary sinus elevation model was selected to evaluate the *in vivo* bone formation induced by SMS hydrogel (Fig. S7). After 12 weeks post-operation, the microCT results were shown in Fig. 9. A-C. There were scattered mineralized nodules in the center of the maxillary sinus elevation region in the SF hydrogel group without new bone formation in most areas. Compared with the SF group, the SMS group had more new bone formation. The number of new bone trabeculae in the SMS group was more prominent than in other groups, as well as the osteogenic ability. The results showed significant statistical differences between the SF and the SMS groups ($p < 0.05$) (Fig. 9. D-F). The volume of new bone in the SMS group was the largest, with significant differences among the groups ($p < 0.01$). The results of VG staining on hard tissue sections showed that the results were consistent with that of microCT. No apparent bone formation in the SF hydrogel group and a large amount of residual silk fibroin hydrogels could be detected. New bone formation was seen in the SMS group, which indicated that the SMS group could also promote bone regeneration *in vivo*. The hydrogel materials of group SMS had mostly degraded, and the defect area was mainly occupied by new bone tissue. On the whole, SMS hydrogel is faster and better than SF hydrogel in promoting bone regeneration in maxillary sinus elevation.

At 4 weeks, tissue sections of the implanted bone interface were treated with Hematoxylin and eosin (HE) staining and Masson's trichrome staining (Fig. 10. A). HE staining showed that there were scattered macrophages around the two groups of hydrogels. Masson's trichrome staining presented the arrangement of collagen fibers around the hydrogels (blue). The collagen fibers around the SF hydrogel were relatively messy. There are many gaps between the fibers, indicating delayed bone regeneration. On the contrary, the collagen fibers around the SMS hydrogel were dense and highly ordered. The distance between them was small, indicating that the mineralized bone was larger than SF hydrogels. Immunohistochemical staining of iNOS (M1) and Arg (M2) was performed on sample sections to characterize the polarization direction of *in vivo* macrophages under the influence of different sample groups (Fig. 10. B). The numbers of iNOS and Arg-positive macrophages in all groups were quantified (Fig. 10. C-E). The SMS group showed a significantly higher ratio of Arg/iNOS than the SF group. In conclusion, *in vivo* inflammatory response analysis at 4 weeks illustrated that SF and SMS had bone immunomodulatory effects on surrounding tissues, while SMS-induced M2 polarization was relatively higher.

HE staining indicated that SF hydrogel still had some residual, while SMS hydrogel basically degraded (Fig. 11. A). The histological image of Masson's trichrome staining showed that SMS was completely surrounded by dense collagen fibers (blue), indicating that the density and quantity of newly formed bone were much higher than those in the SF group (Fig. 11. A). As shown in Fig. 11. B, the VEGF-positive expression in the SMS group was significantly higher than in the SF group, and a dense microvascular network with a tubular structure could be observed. VEGF-positive endothelial cells were reported to enhance the osteogenic differentiation of perivascular bone progenitor cells [55]. Meanwhile, the OCN-positive area was more prominent in the SMS group than in the SF group. This case indicated that SMS helps form more new bones *in vivo*. At 3, 6 and 9 weeks, the newly formed bone was labeled in sequential fluorescence with tetracycline (TE, labeled

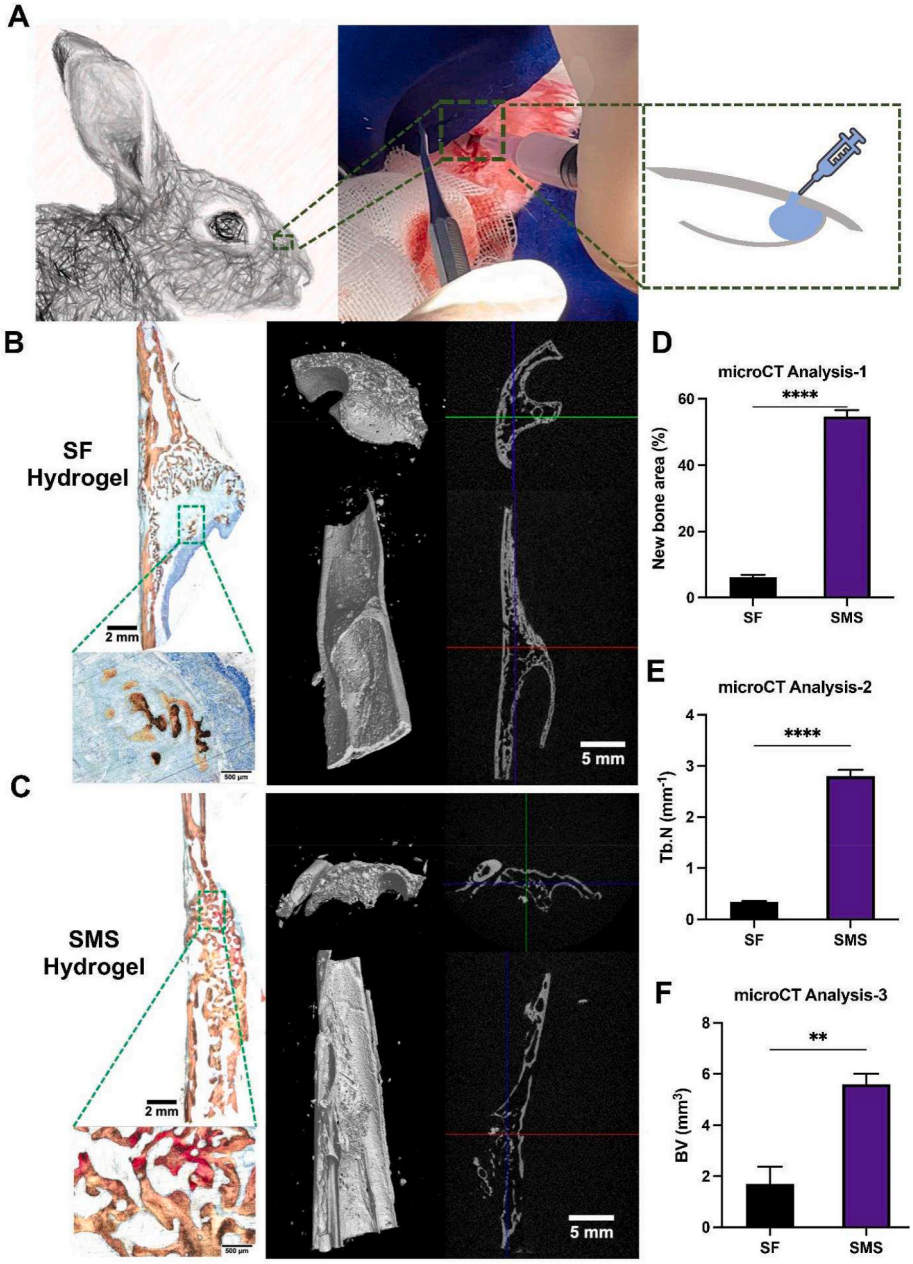

Fig. 9. The effect of SMS hydrogel on bone formation *in vivo* after 12 weeks post-implantation. A) Construction of rabbit maxillary sinus elevation model. B) Van Geison staining and reconstructed 3D images from microCT analysis of hydrogels implanted in rabbit maxillary sinus for 12 weeks. D-F) Quantitative analysis of new bone area, trabecular number (Tb.N) and bone volume (BV). (*$p < 0.05$, **$p < 0.01$, ***$p < 0.005$, ****$p < 0.001$).

yellow), calcein (CA, labeled green) and alizarin red (AL, labeled red), respectively (Fig. 11. C). The fluorescence-labeled areas of the SMS group were remarkably larger than those in the SF group at each time point. In quantitative analysis (Fig. 11 D-F), the area of the remnant materials yielded 50% in the SF group, which was significantly more than that in the SMS group ($p < 0.005$). Oppositely, more than 60% of new bone formation was shown in the SMS group, while only less than 10% of new bone could be found in the SF group. The area of bone stained with TE, CA and AL was measured to understand the new bone formation rate further. The SMS hydrogel showed significant new bone formation at each time point, while the new bone formation rate was significantly faster than the SF group. These data showed that the introduction of SMS could effectively reduce the formation of fibrous tissue. Meanwhile, it promoted vascularised new bone formation. In the immunohistochemical staining of macrophage polarization at 12 weeks (Fig. S8), more positive staining areas of Arg than iNOS could be found in the SMS group, while the positive staining areas of Arg were just similar to iNOS in the SF group.

Rapid bone regeneration will promote the early implantation and weight-bearing of implants, which helps achieve early masticatory function reconstruction and reduce patients' waiting time. High-quality, bone regeneration will also be conducive to the long-term and stable masticatory function of implants. These results jointly demonstrate that SMS achieves the best bone lift effect, thereby confirming the potential of SMS hydrogel for the minimally invasive repair of lacunar bone deficiency. Our results suggest that SMS might be beneficial in regulating bone immune response by promoting M2 polarization of macrophages and achieving vascular bone regeneration.

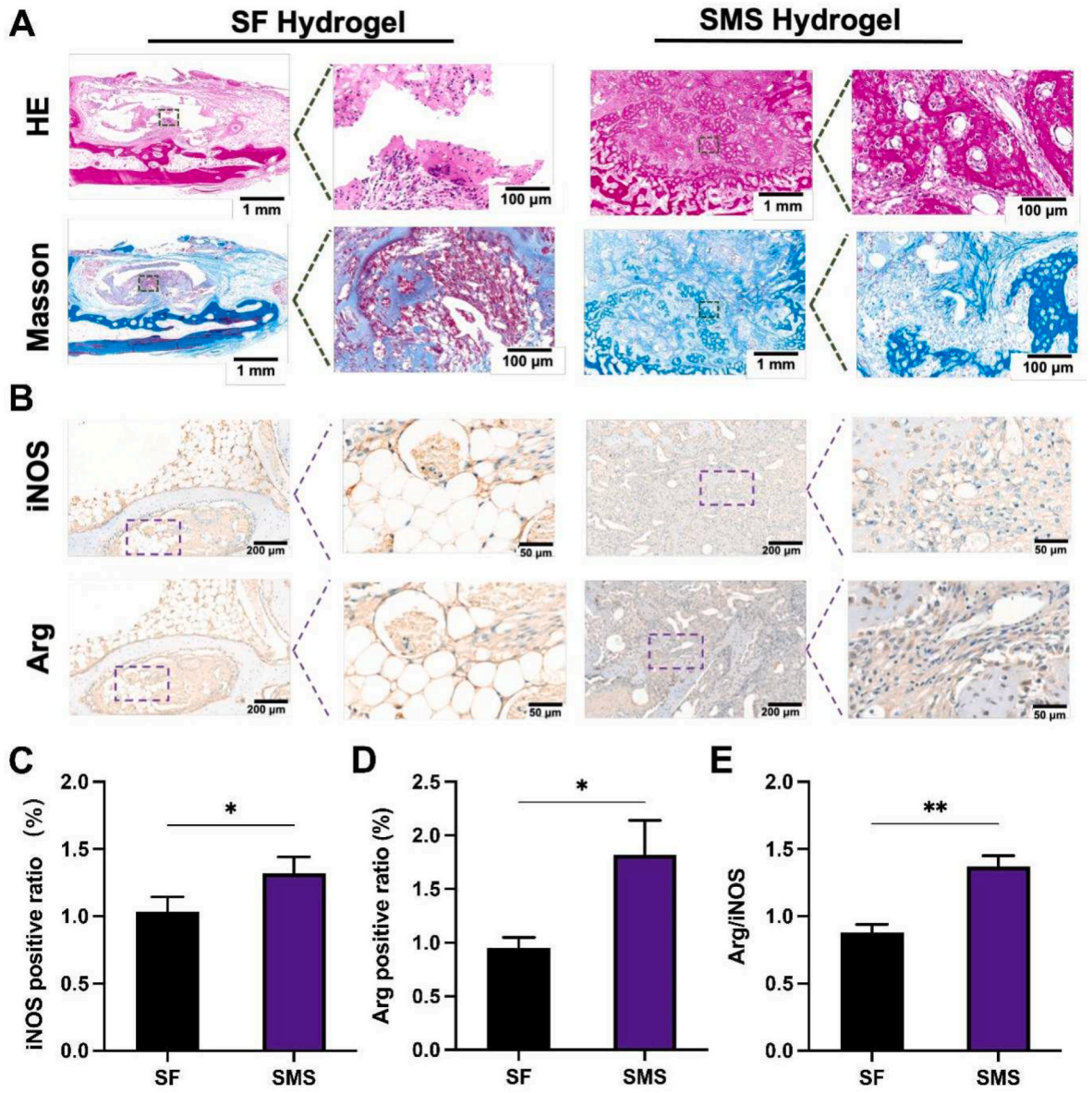

Fig. 10. The histological analysis of the repairment of the defect with different hydrogels after 4-week implantation. A) Hematoxylin and eosin (HE) and Masson's trichrome staining of SF and SMS were injected in a rabbit maxillary sinus for 4 weeks to evaluate inflammatory response. B) Immunohistochemical staining for iNOS and Arg. C-E) Quantitative staining analysis. (*$p < 0.05$, **$p < 0.01$).

3. Conclusion

An injectable adaptive hydrogel was successfully prepared in this study using SF, MBG and SA. The composite SMS hydrogel had a great injectable ability, and attractively SMS hydrogel could be degraded responsibly according to the changes in the microenvironment and could also be enhanced adaptively under the physiological ion concentration. *In vitro,* CCK-8 assay and Live/Dead staining demonstrated that SMS hydrogel presented no obvious cytotoxicity and could promote the proliferation of BMSCs. The expressions of osteogenic genes of BMSCs co-cultured with SMS hydrogel, combined with the ALP activity and the alizarin red staining, outlined that the developed SMS hydrogel could promote osteogenic differentiation of BMSCs *in vitro*. The crosstalk between osteoblasts and macrophages encapsulated that osteoblast differentiation might be related to immune regulation. SMS hydrogel might achieve anti-inflammatory and pro-regenerative effects through MAPK signaling pathway. Three months after the implantation of SMS hydrogel, microCT, and Van Gieson staining envisaged a large new bone area, indicating that SMS obtained good bone regeneration *in vivo*. Thus, SMS hydrogel could be expected to provide a simple, minimally invasive and efficient treatment for the repair of lacunar bone deficiency. In conclusion, the prepared SMS hydrogel is expected to become a new strategy for clinical minimally invasive treatment of lacunar bone deficiency.

4. Experimental section

4.1. Materials

Bombyx mori cocoons were purchased from Jiangsu province, China. $CaCl_2$, sodium alginate and HClwere collected from Aladdin (China). CCK-8, alkaline phosphatase (ALP), and BCA assay kits were ordered from Beyotime Biotechnology Co., Ltd. (Jiangsu, China). FITC-phalloidin and DAPI were purchased from Invitrogen (Carlsbad, CA, USA). Fetal bovine serum (FBS) was obtained from Gibco (USA). DMEM and 100 U/mL penicillin and streptomycin were purchased from Hyclone (South Logan, USA).

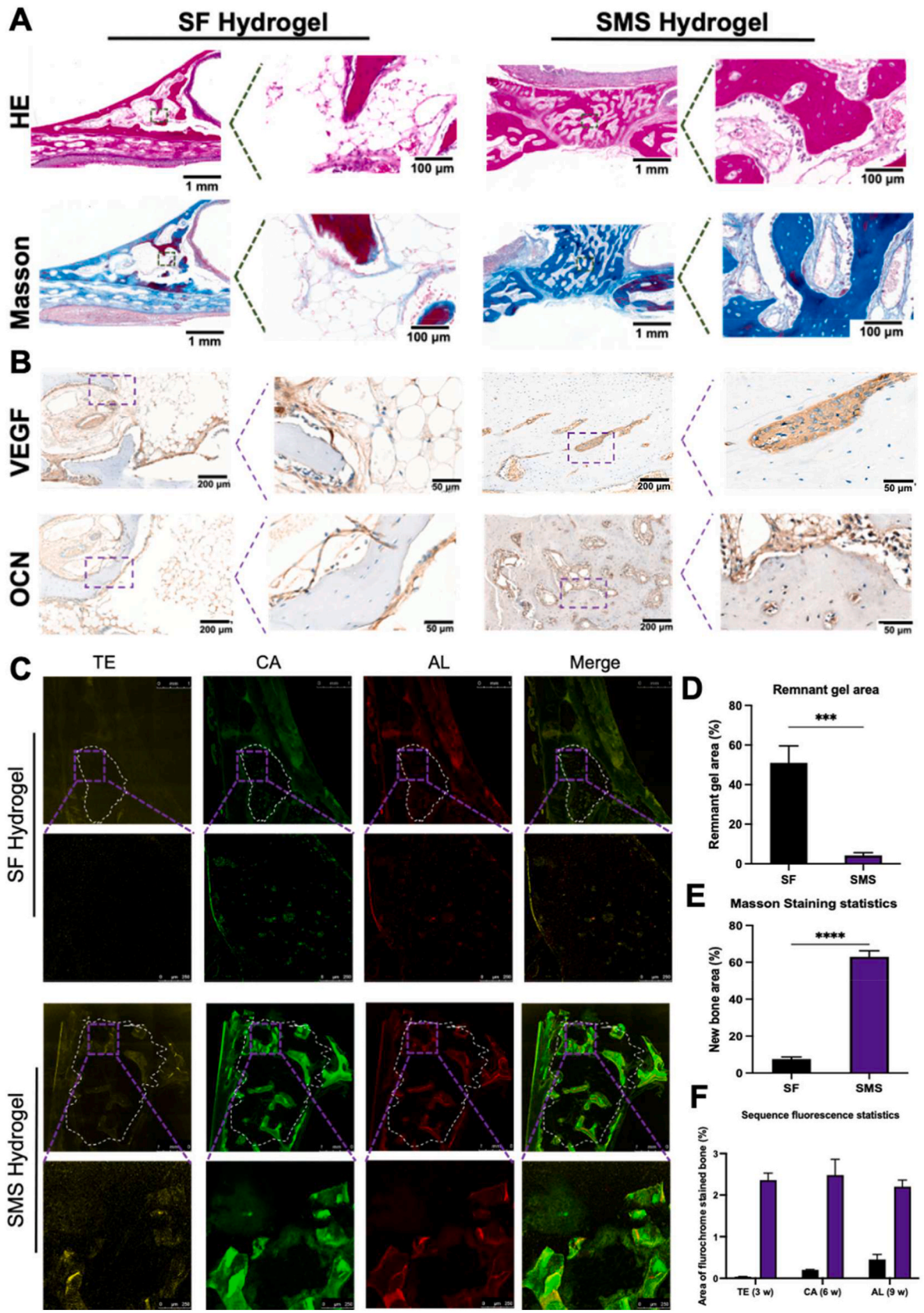

Fig. 11. The histological analysis of the repairment of the defect with different hydrogels after 12-week implantation. A) Hematoxylin and eosin (HE) and Masson's trichrome staining of SF and SMS were injected in a rabbit maxillary sinus for 12 weeks to evaluate bone regeneration. B) Immunohistochemical staining for VEGF and OCN. C) Representative images of sequential fluorescent labeling of the new bone formation by Tetracycline Hydrochloride (TE), Calcein (CA) and Alizarin Red S (AL). (White circle in dotted line: ROI in maxillary sinus). Quantitative analysis of D) remnant gel area in HE staining, E) new bone area in Masson's trichrome staining, and F) new bone formation rate: the proportion of fluorescence area in ROI to the total area of ROI, respectively. (***$p < 0.005$, ****$p < 0.001$).

4.2. Synthesis and characterization of mesoporous bioglass (MBG)

MBG was synthesized as previously described [57]. Briefly, a mixture of TEOS (6.7 g), P123 (4.0 g), TEP (0.36 g), 0.5 M HCl (1.0 g), and Ca $(NO_3)_2{\cdot}4H_2O$ (1.4 g) were prepared in 60 mL ethanol with stirring at 25 °C for 24 h. The resulting sol was treated with an evaporation-induced self-assembly process, followed by drying under a vacuum for 24 h. Then, the obtained materials were calcined at 600 °C in the air for 6 h at a heating rate of 1 °C/min to remove the structure-directing template of P123. The morphologies of MBG samples were observed by SEM and transmission electron microscopy (TEM).

4.3. Preparation of silk fibroin (SF)

Bombyx mori cocoon was washed in 0.5 wt% Na_2CO_3 solutions three times in a 100 °C water bath and then dried at 60 °C for 6 h. The dried silk was dissolved in a ternary solution (molar ratio of $CaCl_2$: water: ethanol = 1:8:2) at 100 °C. The obtained solution was put into a dialysis bag under distilled water for 3 days and then dried and stored after freeze-drying.

4.4. Synthesis of SMS composite hydrogel system

Two premixed solutions were first prepared. Solution I was prepared by dissolving SF (6 wt%) and VC (1 or 1.5 wt%) in deionized water. Solution II was collected by dissolving sodium alginate (SA) (2 wt%) in deionized water and MBG particles were dispersed into the solution at 0.5%, 1%, 1.5% or 2% (w/v). Solution I and Solution II were slowly mixed with stirring. Then the mixture was injected into the mold and stored at 37 °C until gelation.

Pure SF hydrogel was prepared as a control group. 3 wt% SF aqueous solution was treated by ultrasonic for 3 min in an ice water bath, at a rated power of 130 W, amplitude 50%, and rated frequency of 20 kHz. And then, it was poured into the mold at 37 °C until gelation.

4.5. Optimization of SMS composite hydrogel system

4.5.1. Gelation time determination

At 37 °C, the gel solution was poured into the mold and turned every 30 s. The time was recorded once the solution no longer flowed.

4.5.2. Surrounding pH change

The sample was respectively placed in PBS (pH = 7.4) and HCl solution (pH = 6.5) at 0.1 g/mL (w/v) at 37 °C with a shaking speed of 80 rpm. At the pre-determined time point, the pH value of the immersion solution was detected with an acidimeter (S470-USP/EP).

4.5.3. Compressive strength

In order to quantify the compressive strength of SMS composite hydrogels, the hydrogels were prepared into cylindrical (10 mm high × 8 mm diameter) and testified at room temperature on a universal mechanical tester (HY-0230, China). The compression speed was set to 2 mm/min. And then, SMS composite hydrogels with VC content of 1.5% and MBG content of 2% were chosen for future study. For cell culture, antibacterial testing, and *in vivo* studies, hydrogels were prepared in a sterile environment, while each ingredient used to prepare the hydrogel was sterilized by filtration (0.22 μm filter membrane).

4.6. Physical and chemical properties of SMS hydrogel

4.6.1. Injectability and shapeability study of SMS hydrogel

The hydrogel was loaded into a syringe with needle No. 23 and directly squeezed by a needle to the plate or various irregular shapes. Photographs were taken to record the injection process and the appearance of the hydrogel.

4.6.2. Morphology of SMS composite hydrogel

The surface microstructures and cross-sectional morphology of the SMS hydrogel were observed by scanning electron microscope (SEM) (Phenom LE, Phenom-China). The samples were cold-dried in a vacuum for 24 h, sprayed with gold and observed with SEM under an acceleration voltage at 10 kV.

4.6.3. In vitro swelling and degradation properties of the SMS hydrogel

First, the hydrogel sample was weighed and the weight was recorded as W0. Then, the sample was respectively placed in PBS (pH = 7.4) and HCl solution (pH = 6.5) at 0.1 g/mL (w/v) at 37 °C with a shaking speed of 80 rpm. At the pre-determined time point, the sample was taken out and the excess liquid was removed with filter paper, followed by a weight record as Wt. Within 24 h, the swelling rate was calculated at each time point by the formula: S%=(Wt-W0)/W0 × 100%. From 1 to 28 days, the degradation rate was calculated by the formula: D%=(W0-Wt)/W0 × 100%. The morphology of SMS samples degraded after 14 days and 28 days was detected by SEM (Phenom LE, Phenom-China).

4.6.4. Mechanical properties of SMS hydrogel

The samples were prepared into a cylinder (10 mm high × 8 mm diameter) and verified at room temperature on a universal mechanical tester (Shimadzu, Japan). The compression speed was set to 2 mm/min. Rheological properties of hydrogels were studied in terms of a DHR-3 Instruments (DE, USA). All experiments were carried out at 25.0 °C using 35.0 mm parallel plates with a plate gap of 1.0 mm. Frequency scanning was performed at an oscillation frequency of 0.1–100.0 rad s^{-1} at the 1.0% strain level. The storage modulus (G′) and loss modulus (G″) were measured. For adaptability determination *in vitro*, 1 mM $CaCl_2$ solution was selected to mimic the physiological Ca^{2+} concentration in the bone microenvironment [30], in which SMS hydrogel samples were immersed for 24 h, followed by compressive strength detection, respectively.

4.6.5. In vitro release

0.5 g hydrogel was immersed in 20 mL deionized water at 37 °C with stirring at a speed of 100 rpm. At a pre-determined time-point, the concentrations of the released ions were measured by inductively coupled plasma mass spectrometry (ICP, Agilent 710, California, USA). Each sample was tested in triplicate.

4.7. Effect of SMS hydrogel on osteogenic differentiation in vitro

4.7.1. Isolation and culture of rat bone marrow mesenchymal stem cells (BMSCs)

All experimental protocols regarding the use of animals in this study were approved by the Institutional Animal Care and Use Committee and followed the procedure for Animal Experimental Ethical Inspection of the Ninth People's Hospital, affiliated with Shanghai Jiao Tong University School of Medicine. Animal license No. is SCXK (Shanghai) 2012–0007. 8 male SD rats, aged 4 weeks and weighing 200 ± 20 g. Briefly, the bone marrow cavity was washed with DMEM medium from the femur and cultured in the incubator at 37 °C and 5% CO_2. The medium was changed every 3 days. BMSCs of passages 2 to 4 were selected for this study.

4.7.2. Morphological observation of BMSC on the surface of SMS hydrogel

SMS hydrogels or SF hydrogels were prepared under sterile conditions with diameters of 10 mm and 1 mm discs. 1.0×10^5 BMSCs were seeded on hydrogel samples for 12 h. All samples were removed and fixed with 4% glutaraldehyde at room temperature for 15 min. Cellular F-actin was stained with FITC-phalloidin for 1 h at 37 °C for cytoskeleton observation. Subsequently, nuclei were stained with DAPI for 10 min. Cell morphology was observed using a confocal laser scanning microscope (CLSM, Leica, Wetzlar, Germany).

4.7.3Detection of cell viability of SMS hydrogel

5×10^3 BMSCs were seeded on 100 μL gel in 96-well plates and cultured in a 5% CO_2-conditioned incubator. The medium containing CCK-8 working solution was added after 1, 3 and 7 days. After incubation at 37 °C for 2 h, the absorbance was measured at 450 nm (Safire, TECAN). To investigate the effect of the released ingredients from hydrogels on BMSCs viability and exclude the influence of surface morphology, we used a transwell co-culture system and studied *in vitro* biological properties of SMS hydrogel. BMSCs were incubated in 24-well plates with a density of 2×10^5 cells/well. 200 μL hydrogel was prepared in a transwell chamber (membrane pore size: 0.4 mm) and employed to co-culture with the cells. The medium containing CCK-8 working solution was added after 1, 3 and 7 days. After incubation at 37 °C for 2 h, the absorbance was measured at 450 nm. A live/dead staining approach was employed to evaluate the activity of cells seeded on the SMS hydrogel system. 1×10^4 BMSCs were seeded on 200 μL hydrogel and cultured for 1 and 7 days. The red cells were dead, while the green ones were living cells. The live/dead staining was operated according to the instructions. The stained cells were observed using CLSM (Leica, Wetzlar, Germany).

4.8. Effect of SMS composite hydrogel on BMSCs differentiation and mineralization

4.8.1. Effect of composite hydrogel on alkaline phosphatase (ALP) activity of BMSCs

The BMSCs suspension with a density of 5×10^4 cells/mL was seeded onto 150 μL composite hydrogel in a cell culture dish with a 10 mm diameter glass bottom, mainly to analyze the osteogenic effect of the composites. ALP immunofluorescence staining was investigated at 7 days. BMSCs were incubated in 24 well plates with a density of 1×10^5 cells/well. 200 μL hydrogel was prepared in a transwell chamber (membrane pore size: 0.4 mm) and employed to co-culture with the cells. After 3 days and 7 days of co-culture, the ALP staining and the semi-quantity of ALP activity in BMSCs were carried out. The semi-quantitative value of ALP was measured by a BCA kit (Biyuntian, China) according to the company's experimental procedures. Besides, 405 nm wavelength was employed to detect the absorbance value on the microplate. The expression of ALP was stained with a BCIP/NBT alkaline phosphatase staining kit (Biyuntian, China) according to the manufacturer's instructions and then observed under an inverted fluorescence microscope (Ti–U, Nikon, Japan).

4.8.2. Alizarin red staining in vitro mineralization experiment

In the 24-well plate, 1×10^5 cells were incubated in each well. Besides, 200 μL hydrogel was prepared in a cell culture chamber (pore size 0.4 μm). The transwell plate was employed to co-culture the materials with cells. After 21 days and 28 days of culture, the hydrogel and culture medium were removed with the cells fixed at room temperature for 10 min at 4% paraformaldehyde and stained with 1% alizarin red dye. Finally, the cells were washed to remove the unconjugated dyes on the surface. The cells were observed and photographed under an inverted microscope (Ti–U, Nikon, Japan). Cetylpyridinium chloride was added to the culture plate stained with alizarin red. We concluded that cetylpyridinium chloride could dissolve alizarin red combined with a calcium salt. The supernatant was collected and the absorbance was detected at a 590 nm wavelength. In the meantime, the total protein content was determined as above.

4.8.3. The expression of osteogenic-related genes detected by qRT-PCR

BMSCs were seeded in 6-well plates with a density of 5×10^5 cells/well. In the transwell chamber (0.4 mm), 400 μL hydrogels were prepared. The materials were co-cultured with cells by using the transwell system. LightCycle480 (Roche, Switzerland) was used for qRT-PCR detection after culture for 7 and 14 days. The cells cultured in a blank medium without a gel chamber were employed as the blank control group (CON). GAPDH was selected as the internal reference. The relative gene expression of the target gene corresponding to each group of samples was taken as the reference value (set as 1). On top of that, the multiple changes based on it were recorded as mean ± standard deviation (SD). The primer sequences of marker genes are shown in Table S1.

4.9. Immune response of macrophages

4.9.1Macrophage cell culture

RAW 264.7 cells (murine-derived macrophage) were cultured on the surface of hydrogels or cell culture plate (control group) at 37 °C and 5% CO_2 in DMEM medium with 10% FBS and 1% penicillin/streptomycin. After 24 h of culture, cellular F-actin was stained with FITC-phalloidin, while nuclei were stained with DAPI. The macrophage morphology was observed using a CLSM (Leica, Wetzlar, Germany).

For the cell proliferation test, 500 μL hydrogel was prepared in the lower chamber of the 6-well plate, with a 2 mL addition of the culture medium. After insert of the upper chamber with RAW 264.7 cells at a seeding density of 9×10^4/well, 1 mL culture medium was added. For 1, 3, and 7 days, cell proliferation of RAWs in the upper chamber was detected by CCK8 assay according to the manufacturer's instructions.

4.9.2. Inflammation-related gene expression

After co-cultured with hydrogels for 3 and 7 days, the expression levels of inflammation-related genes of RAW 264.7 cells, including TNF-α, IL-1β, TGF-β and IL-10, were detected using qRT-PCR following the same procedures as described above. Primer sequences are listed in Table S1.

4.9.3. Osteogenesis-immune crosstalk between macrophages and BMSCs

In order to investigate the effect of the co-culture of RAWs and hydrogel on the osteogenic differentiation of BMSCs, 500 μL hydrogel was prepared in the lower chamber of the 6-well plate, with seeding of RAWs on the gel surface at a density of 2×10^5/well. Then, 2 mL of the culture medium was added. After insert of the upper chamber with BMSCs seeding at a density of 5×10^4/well, 1 mL culture medium was added. For 7 and 14 days, the expressions of osteogenic related genes of BMSCs in the upper chamber were detected by qRT-PCR. In order to investigate the effect of the co-culture of BMSCs and hydrogel on the polarization of RAWs, 500 μL hydrogel was prepared in the lower chamber of the 6-well plate, with seeding of BMSCs on the gel surface at a density of 1.5×10^5 per well. Then, 2 mL of the culture medium was added. After insert of the upper chamber with RAWs seeding at a density of 9×10^4/well, 1 mL culture medium was added. For 3 and 7 days, the expressions of inflammation-related genes of RAWs in the upper chamber were detected by qRT-PCR.

4.10. Effect of SMS hydrogel on angiogenesis in vitro

4.10.1. Cell culture

HUVECs were cultured in Dulbecco's Modified Eagle's Medium (DMEM, Hyclone, USA), which was supplemented with 10% fetal bovine serum (FBS, GIBCO, USA), 100 U/mL penicillin (Hyclone, USA) and 100 μg/mL streptomycin, in 37 °C, 5%CO_2.

4.10.2. Cell migration

200 μL hydrogel was put in each 24-well transwell lower chamber with 400 μL DMEM. 5×10^3 cells in 100 μL cell suspension were added to each transwell upper chamber. After 12 h of culture, the Transwell chamber was taken out, washed with PBS, and gently wiped off the upper layer of non-migrated cells with a cotton swab. The cells were fixed with 4% paraformaldehyde, stained with 1% crystal violet solution for 20 min, observed, and photographed under a microscope (Ti–U, Nikon, Japan).

4.10.3. Tube forming experiment

50 μL matrigel (BD Biosciences, USA) was transferred to each well of a 96-well plate and then cultured in a 37 °C incubator for 30 min to form a gel. Then HUVECs co-cultured with different hydrogels in advance at a density of 1×10^5 cells/well were added and incubated on the surface of the matrigel. After incubation at 37 °C for 6 h, the cells were fixed with 4% paraformaldehyde and photographed under a microscope (Ti–U, Nikon, Japan). Image J was used to calculate the number of circular structures, the number of nodes, and the length of tubular branches.

4.11. Antibacterial activity of SMS hydrogels

In this study, gram-negative *E. coli* and gram-positive *S. aureus* were selected to evaluate the antibacterial activity of different hydrogels. Briefly, 0.5 g hydrogel was incubated with 2 mL bacterial suspension (10^6 CFU/mL) at 37 °C for 10 h, followed by three times of gentle washing with PBS and observation under SEM. In addition, the sample was also washed in an ultrasonic bath (50 Hz, 10 min) to release bacteria firmly adhering to the surface. The suspension was continuously diluted and incubated on trypsin soybean agar (TSA). After incubation at 37 °C for 10 h, digital photos of the plate were taken, and the colonies on TSA were counted.

4.12. Analysis of the possible regulation mechanism related to SMS hydrogels

BMSCs were incubated in 6-well plates with a seeding density of 5×10^5 cells/well. The materials were co-cultured with cells by using the transwell system. In the culture chamber (membrane pore size: 0.4 μm), 400 μL hydrogel was placed. After 5 min of culture with different hydrogels, the cells were collected for Western blot assay. Furthermore, BMSCs were co-cultured with SMS hydrogel and 20×10^{-6} M PD98059 (Selleck, China) or 20×10^{-6} M SP600125 (Selleck, China). As a control group, BMSCs were co-cultured with SMS hydrogel only. Phosphorylation of Erk1/2 and JNK was detected by Western blot. Osteogenic differentiation was evaluated based on ALP staining.

Total protein was extracted with RIPA Lysis and Extraction Buffer (Thermo Fisher Scientific). According to the manufacturer's instructions, the BCA Protein Assay Kit was employed to determine the protein concentration. Then the protein extracts were separated by SDS-PAGE and transferred onto a PVDF membrane (Millipore, Billerica, MA, USA). Membranes were blocked with 5% BSA and incubated with primary antibodies against p-JNK (Abcam, 1/10000), JNK (Abcam, 1/10000), p-Erk1/2 (Abcam, 1/10000), Erk1/2 (Abcam, 1/10000), GAPDH (CST, 1/1000), for 4 °C overnight. Then, the membranes were hatched with horseradish peroxidase-labeled secondary antibodies for 2 h at room temperature. The membrane was then washed with Tris-buffered saline and developed using an enhanced chemiluminescence detection system with exposure to FluorChem™ HD2 (Cell Biosciences, Inc., Santa Clara, CA, USA).

4.13. Effect of SMS hydrogel on bone regeneration in vivo

4.13.1. The operation of rabbit maxillary sinus elevation

12 male New Zealand white rabbits with 2.5 kg weight were employed in this study (Animal license No. SCXK (Shanghai) 2012–0007). After anesthetization, a 2.5-cm long vertical incision was made on the nasal face along the midline. A bone window with a diameter of 5 mm was prepared on both sides with a grinding head, 2 cm before the nasal frontal suture and 0.5 cm outside the midline. The maxillary sinus membrane was gently pushed out with a space of 8 mm × 3 mm × 5 mm, in which 200 μL of different groups of hydrogels were filled. Finally, the periosteum was closed and sutured, and the incision was sutured.

4.13.2. Sequential fluorescent labeling

Polychromatic sequential fluorescence labeling was performed on rabbits to evaluate the new bone formation and mineralization rate induced by different hydrogels *in vivo*. 25 mg/kg tetracycline hydrochloride (TE, sigma, USA), 20 mg/kg calcein (CA, sigma, USA), and 30 mg/kg Alizarin Red S (AL, sigma, USA) were injected intraperitoneally at 3-, 6- and 9-week post-operation, respectively.

4.13.3. MicroCT detection of new bone formation in the maxillary sinus elevation area

At pre-determined time points, the rabbits were sacrificed. The maxilla with the material was removed and fixed in 10% neutral formalin. MicroCT (μCT50, SCANCO) scanning was employed to observe the new bone in the maxillary sinus region. The volume of new bone and the number of new bone trabeculae were also quantitively analyzed.

4.13.4. Histological and histomorphometric observation

The samples were taken at 4- and 12-week post-operation, respectively. Half of the samples were decalcified, embedded in paraffin, and cut into 4 μm slices, followed by HE and Masson's trichrome staining. The other half samples were dehydrated, embedded in polymethylmethacrylate (PMMA), and cut into sections using a slicer (Leica, Germany). These non-decalcified sections were observed by CLSM for fluorescence labeling and further treated with Von Gieson staining for bone formation observation. Furthermore, decalcified sections of 4 and 12-week samples were treated with iNOS (Abcam, USA) and Arg (Abcam, USA) immunohistochemical staining, while OCN (Abcam, USA) and VEGF (Abcam, USA) immunohistochemical staining for 12-week samples. All images were photographed under a microscope (Ti–U, Nikon, Japan) and analyzed by Image J software.

4.14. Statistical analysis

All quantitative data are the average of three independent experiments and are presented as the mean ± SD. All data were analyzed by Origin 9.0. $p < 0.05$ was considered a significant difference. After testing the normality, statistical analysis was performed using a one-way analysis of variance followed by the least significant difference test.

Funding

This research was funded by the National Natural Science Foundation of China (Nos. 82130027, 82100963, 82270953, 81991505 and 81921002), Shanghai Rising-Star Program (21QA1405400), Natural Science Foundation of Shanghai (22ZR1436400), and the Innovative Research Team of High-Level Local Universities in Shanghai.

Ethics approval and consent to participate

All experimental protocols regarding the use of animals in this study were approved by the Institutional Animal Care and Use Committee and followed the procedure for Animal Experimental Ethical Inspection of the Ninth People's Hospital, affiliated with Shanghai Jiao Tong University School of Medicine. Animal license No. is SCXK (Shanghai) 2012–0007.

CRediT authorship contribution statement

Ao Zheng: Conceptualization, Methodology, Data curation, Writing – original draft, All authors have read and agreed to the published version of the manuscript. **Xiao Wang:** Methodology, Data curation, Writing – review & editing, All authors have read and agreed to the published version of the manuscript. **Xianzhen Xin:** Writing – review & editing, All authors have read and agreed to the published version of the manuscript. **Lingjie Peng:** Project administration. **Tingshu Su:** Software, Funding acquisition, All authors have read and agreed to the

published version of the manuscript. **Lingyan Cao:** Conceptualization, Writing – review & editing, Funding acquisition, All authors have read and agreed to the published version of the manuscript. **Xinquan Jiang:** Conceptualization, Writing – review & editing, Funding acquisition, All authors have read and agreed to the published version of the manuscript.

Acknowledgements

Ao Zheng and Xiao Wang contributed equally to this work.

Appendix A. Supplementary data

Supplementary data to this article can be found online at https://doi.org/10.1016/j.bioactmat.2022.08.031.

References

[1] T. Liu, J. Xu, X. Pan, Z. Ding, H. Xie, X. Wang, H. Xie, Advances of adipose-derived mesenchymal stem cells-based biomaterial scaffolds for oral and maxillofacial tissue engineering, Bioact. Mater. 6 (8) (2021) 2467–2478, https://doi.org/10.1016/j.bioactmat.2021.01.015.

[2] Z.M. Wu, X.G. Zhang, C. Zheng, C.X. Li, S.M. Zhang, R.N. Dong, D.M. Yu, Disulfide-crosslinked chitosan hydrogel for cell viability and controlled protein release, Eur. J. Pharmaceut. Sci. 37 (3) (2009) 198–206, https://doi.org/10.1016/j.ejps.2009.01.010.

[3] F.G. Omenetto, D.L. Kaplan, New opportunities for an ancient material, Science 329 (5991) (2010) 528–531, https://doi.org/10.1126/science.1188936.

[4] Y. Wang, D.D. Rudym, A. Walsh, L. Abrahamsen, H.J. Kim, H.S. Kim, C. Kirker-Head, D.L. Kaplan, In vivo degradation of three-dimensional silk fibroin scaffolds, Biomaterials 29 (24–25) (2008) 3415–3428, https://doi.org/10.1016/j.biomaterials.2008.05.002.

[5] Y. Li, Z. Liu, Y. Tang, Q. Fan, W. Feng, C. Luo, G. Dai, Z. Ge, J. Zhang, G. Zou, Y. Liu, N. Hu, W. Huang, Three-dimensional silk fibroin scaffolds enhance the bone formation and angiogenic differentiation of human amniotic mesenchymal stem cells: a biocompatibility analysis, Acta Biochim. Biophys. Sin. 52 (6) (2020) 590–602, https://doi.org/10.1093/abbs/gmaa042.

[6] H.J. Jin, D.L. Kaplan, Mechanism of silk processing in insects and spiders, Nature 424 (6952) (2003) 1057–1061, https://doi.org/10.1038/nature01809.

[7] W. Zhang, X. Wang, S. Wang, J. Zhao, L. Xu, C. Zhu, D. Zeng, J. Chen, Z. Zhang, D. L. Kaplan, X. Jiang, The use of injectable sonication-induced silk hydrogel for VEGF (165) and BMP-2 delivery for elevation of the maxillary sinus floor, Biomaterials 32 (35) (2011) 9415–9424, https://doi.org/10.1016/j.biomaterials.2011.08.047.

[8] P.A. Panteli, C.S. Patrickios, Multiply interpenetrating polymer networks: preparation, mechanical properties, and applications, Gels 5 (3) (2019) 36, https://doi.org/10.3390/gels5030036.

[9] K. Ziv, H. Nuhn, Y. Ben-Haim, L.S. Sasportas, P.J. Kempen, T.P. Niedringhaus, M. Hrynyk, R. Sinclair, A.E. Barron, S.S. Gambhir, A tunable silk–alginate hydrogel scaffold for stem cell culture and transplantation, Biomaterials 35 (12) (2014) 3736–3743, https://doi.org/10.1016/j.biomaterials.2014.01.029.

[10] Y. Cao, X. Shen, Y. Chen, J. Guo, Q. Chen, X. Jiang, pH-induced self-assembly and capsules of sodium alginate, Biomacromolecules 6 (4) (2005) 2189–2196, https://doi.org/10.1021/bm0501510.

[11] P. Garidel, M. Rappolt, A.B. Schromm, J. Howe, K. Lohner, J. Andra, M.H. Koch, K. Brandenburg, Divalent cations affect chain mobility and aggregate structure of lipopolysaccharide from Salmonella Minnesota reflected in a decrease of its biological activity, Biochim. Biophys. Acta 1715 (2) (2005) 122–131, https://doi.org/10.1016/j.bbamem.2005.07.013.

[12] M. Kamitakahara, C. Ohtsuki, T. Miyazaki, Review paper: behavior of ceramic biomaterials derived from tricalcium phosphate in physiological condition, J. Biomater. Appl. 23 (3) (2008) 197–212, https://doi.org/10.1177/0885328208096798.

[13] C. Mao, X. Chen, Q. Hu, G. Miao, C. Lin, Acute toxicity and in vivo biodistribution of monodispersed mesoporous bioactive glass spheres in intravenously exposed mice, Mater. Sci. Eng. C-Mater. Biol. Appl. 58 (2016) 682–691, https://doi.org/10.1016/j.msec.2015.09.002.

[14] J.R. Jones, Reprint of: review of bioactive glass: from Hench to hybrids, Acta Biomater. 23 (Suppl) (2015) S53–S82, https://doi.org/10.1016/j.actbio.2015.07.019.

[15] S.A.L. Barros, D.G. Soares, M.L. Leite, F.G. Basso, C.A.S. Costa, G.L. Adabo, Influence of zirconia-coated bioactive glass on gingival fibroblast behavior, Braz. Dent. J. 30 (4) (2019) 333–341, https://doi.org/10.1590/0103-6440201902417.

[16] L. Wang, J. Wang, X. Zhou, J. Sun, B. Zhu, C. Duan, P. Chen, X. Guo, T. Zhang, H. Guo, A new self-healing hydrogel containing hucMSC-derived exosomes promotes bone regeneration, Front. Bioeng. Biotechnol. 8 (2020), 564731, https://doi.org/10.3389/fbioe.2020.564731.

[17] D.S. Garske, K. Schmidt-Bleek, A. Ellinghaus, A. Dienelt, L. Gu, D.J. Mooney, G. N. Duda, A. Cipitria, Alginate hydrogels for in vivo bone regeneration: the immune competence of the animal model matters, Tissue Eng. 26 (15–16) (2020) 852–862, https://doi.org/10.1089/ten.TEA.2019.0310.

[18] P. Zhou, X. Xie, D.P. Knight, X.H. Zong, F. Deng, W.H. Yao, Effects of pH and calcium ions on the conformational transitions in silk fibroin using 2D Raman correlation spectroscopy and 13C solid-state NMR, Biochem. 43 (35) (2004) 11302–11311, https://doi.org/10.1021/bi049344i.

[19] L. Colombo, L. Zoia, M.B. Violatto, S. Previdi, L. Talamini, L. Sitia, F. Nicotra, M. Orlandi, M. Salmona, C. Recordati, P. Bigini, B. La Ferla, Organ distribution and bone tropism of cellulose nanocrystals in living mice, Biomacromolecules 16 (9) (2015) 2862–2871, https://doi.org/10.1021/acs.biomac.5b00805.

[20] J. He, G. Hwang, Y. Liu, L. Gao, L. Kilpatrick-Liverman, P. Santarpia, X. Zhou, H. Koo, l-Arginine modifies the exopolysaccharide matrix and thwarts Streptococcus mutans outgrowth within mixed-species oral biofilms, J. Bacteriol. 198 (19) (2016) 2651–2661, https://doi.org/10.1128/jb.00021-16.

[21] B. Horev, M.I. Klein, G. Hwang, Y. Li, D. Kim, H. Koo, D.S. Benoit, pH-activated nanoparticles for controlled topical delivery of farnesol to disrupt oral biofilm virulence, ACS Nano 9 (3) (2015) 2390–2404, https://doi.org/10.1021/nn507170s.

[22] A.F. Radovic-Moreno, T.K. Lu, V.A. Puscasu, C.J. Yoon, R. Langer, O.C. Farokhzad, Surface charge-switching polymeric nanoparticles for bacterial cell wall-targeted delivery of antibiotics, ACS Nano 6 (5) (2012) 4279–4287, https://doi.org/10.1021/nn3008383.

[23] S. Schlafer, M.K. Raarup, R.L. Meyer, D.S. Sutherland, I. Dige, J.R. Nyengaard, B. Nyvad, pH landscapes in a novel five-species model of early dental biofilm, PLoS One 6 (9) (2011), e25299, https://doi.org/10.1371/journal.pone.0025299.

[24] J. Wu, K. Zheng, X. Huang, J. Liu, H. Liu, A.R. Boccaccini, Y. Wan, X. Guo, Z. Shao, Thermally triggered injectable chitosan/silk fibroin/bioactive glass nanoparticle hydrogels for in-situ bone formation in rat calvarial bone defects, Acta Biomater. 91 (2019) 60–71, https://doi.org/10.1016/j.actbio.2019.04.023.

[25] X. Chen, Y. Zhao, S. Geng, R.J. Miron, Q. Zhang, C. Wu, Y. Zhang, In vivo experimental study on bone regeneration in critical bone defects using PIB nanogels/boron-containing mesoporous bioactive glass composite scaffold, Int. J. Nanomed. 10 (2015) 839–846, https://doi.org/10.2147/IJN.S69001.

[26] T. Sun, R. Liu, X. Liu, X. Feng, Y. Zhang, R. Lai, The biocompatibility of dental graded nano-glass-zirconia material after aging, Nanoscale Res. Lett. 13 (1) (2018) 61, https://doi.org/10.1186/s11671-018-2479-4.

[27] F. Liu, Y. Liu, X. Li, X. Wang, D. Li, S. Chung, C. Chen, I.S. Lee, Osteogenesis of 3D printed macro-pore size biphasic calcium phosphate scaffold in rabbit calvaria, J. Biomater. Appl. 33 (9) (2019) 1168–1177, https://doi.org/10.1177/0885328218825177.

[28] M. Zhang, X. Chen, X. Pu, X. Liao, Z. Huang, G. Yin, Dissolution behavior of CaO-MgO-SiO2-based multiphase bioceramic powders and effects of the released ions on osteogenesis, J. Biomed. Mater. Res., Part A 105 (11) (2017) 3159–3168, https://doi.org/10.1002/jbm.a.36154.

[29] T. Xin, Y. Gu, R. Cheng, J. Tang, Z. Sun, W. Cui, L. Chen, Inorganic strengthened hydrogel membrane as regenerative periosteum, ACS Appl. Mater. Interfaces 9 (47) (2017) 41168–41180, https://doi.org/10.1021/acsami.7b13167.

[30] B. Liu, X. Gu, Q. Sun, S. Jiang, J. Sun, K. Liu, F. Wang, Y. Wei, Injectable in situ induced robust hydrogel for photothermal therapy and bone fracture repair, Adv. Funct. Mater. 31 (19) (2021), 2010779, https://doi.org/10.1002/adfm.202010779.

[31] L. Chu, H. Gao, T. Cheng, Y. Zhang, J. Liu, F. Huang, C. Yang, L. Shi, J. Liu, A charge-adaptive nanosystem for prolonged and enhanced in vivo antibiotic delivery, Chem. Commun. 52 (37) (2016) 6265–6268, https://doi.org/10.1039/c6cc01269h.

[32] G. Walters, I. Pountos, P.V. Giannoudis, The cytokines and micro-environment of fracture haematoma: current evidence, J. Tissue Eng. Regen. Med. 12 (3) (2018) e1662–e1677, https://doi.org/10.1002/term.2593.

[33] S. Herber, J. Bomer, W. Olthuis, P. Bergveld, A. van den Berg, A miniaturized carbon dioxide gas sensor based on sensing of pH-sensitive hydrogel swelling with a pressure sensor, Biomed. Microdevices 7 (3) (2005) 197–204, https://doi.org/10.1007/s10544-005-3026-5.

[34] Y. Wang, G. He, Z. Li, J. Hua, M. Wu, J. Gong, J. Zhang, L.T. Ban, L. Huang, Novel biological hydrogel: swelling behaviors study in salt solutions with different ionic valence number, Polymers 10 (2) (2018), https://doi.org/10.3390/polym10020112.

[35] M. Yoshinari, T. Hayakawa, K. Matsuzaka, T. Inoue, Y. Oda, M. Shimono, T. Ide, T. Tanaka, Oxygen plasma surface modification enhances immobilization of simvastatin acid, Biomed. Res. 27 (1) (2006) 29–36, https://doi.org/10.2220/biomedres.27.29.

[36] L. Cao, J. Wang, J. Hou, W. Xing, C. Liu, Vascularization and bone regeneration in a critical sized defect using 2-N,6-O-sulfated chitosan nanoparticles incorporating BMP-2, Biomaterials 35 (2) (2014) 684–698, https://doi.org/10.1016/j.biomaterials.2013.10.005.

[37] Y. Zhu, Z. Ma, L. Kong, Y. He, H.F. Chan, H. Li, Modulation of macrophages by bioactive glass/sodium alginate hydrogel is crucial in skin regeneration enhancement, Biomaterials 256 (2020), 120216, https://doi.org/10.1016/j.biomaterials.2020.120216.

[38] N. Farfan, J. Carril, M. Redel, M. Zamorano, M. Araya, E. Monzon, R. Alvarado, N. Contreras, A. Tapia-Bustos, M.E. Quintanilla, F. Ezquer, J.L. Valdes, Y. Israel, M. Herrera-Marschitz, P. Morales, Intranasal administration of mesenchymal stem cell secretome reduces hippocampal oxidative stress, neuroinflammation and cell death, improving the behavioral outcome following perinatal asphyxia, Int. J. Mol. Sci. 21 (20) (2020) 7800, https://doi.org/10.3390/ijms21207800.

[39] S. Nozawa, S. Narisawa, R. Iizuka, T. Fukasawa, T. Kohji, P.K. Nakane, K. Hirano, J. L. Millan, The mechanism of placental alkaline phosphatase induction in vitro, Cell Biochem. Funct. 7 (3) (1989) 227–232, https://doi.org/10.1002/cbf.290070312.

[40] K. Gomathi, N. Akshaya, N. Srinaath, A. Moorthi, N. Selvamurugan, Regulation of Runx2 by post-translational modifications in osteoblast differentiation, Life Sci. 245 (2020), 117389, https://doi.org/10.1016/j.lfs.2020.117389.
[41] T.A. Wynn, K.M. Vannella, Macrophages in tissue repair, regeneration, and fibrosis, Immunity 44 (3) (2016) 450–462, https://doi.org/10.1016/j.immuni.2016.02.015.
[42] R.M. Boehler, R. Kuo, S. Shin, A.G. Goodman, M.A. Pilecki, R.M. Gower, J. N. Leonard, L.D. Shea, Lentivirus delivery of IL-10 to promote and sustain macrophage polarization towards an anti-inflammatory phenotype, Biotechnol. Bioeng. 111 (6) (2014) 1210–1221, https://doi.org/10.1002/bit.25175.
[43] S.B. Singh, H.C. Lin, Role of intestinal alkaline phosphatase in innate immunity, Biomolecules 11 (12) (2021) 1784, https://doi.org/10.3390/biom11121784.
[44] B.N. Brown, B.D. Ratner, S.B. Goodman, S. Amar, S.F. Badylak, Macrophage polarization: an opportunity for improved outcomes in biomaterials and regenerative medicine, Biomaterials 33 (15) (2012) 3792–3802, https://doi.org/10.1016/j.biomaterials.2012.02.034.
[45] A. Mantovani, S.K. Biswas, M.R. Galdiero, A. Sica, M. Locati, Macrophage plasticity and polarization in tissue repair and remodelling, J. Pathol. 229 (2) (2013) 176–185, https://doi.org/10.1002/path.4133.
[46] L. Ouyang, J. Cao, Q. Dai, D. Qiu, New insight of immuno-engineering in osteoimmunomodulation for bone regeneration, Regen. Ther. 18 (2021) 24–29, https://doi.org/10.1016/j.reth.2021.03.003.
[47] O.R. Mahon, D.C. Browe, T. Gonzalez-Fernandez, P. Pitacco, I.T. Whelan, S. Von Euw, C. Hobbs, V. Nicolosi, K.T. Cunningham, K.H.G. Mills, D.J. Kelly, A. Dunne, Nano-particle mediated M2 macrophage polarization enhances bone formation and MSC osteogenesis in an IL-10 dependent manner, Biomaterials 239 (2020), 119833, https://doi.org/10.1016/j.biomaterials.2020.119833.
[48] J. Zhang, Q. Wu, C. Yin, X. Jia, Z. Zhao, X. Zhang, G. Yuan, H. Hu, Q. Zhao, Sustained calcium ion release from bioceramics promotes CaSR-mediated M2 macrophage polarization for osteoinduction, J. Leukoc. Biol. 110 (3) (2021) 485–496, https://doi.org/10.1002/jlb.3ma0321-739r.
[49] D.O. Freytes, J.W. Kang, I. Marcos-Campos, G. Vunjak-Novakovic, Macrophages modulate the viability and growth of human mesenchymal stem cells, J. Cell. Biochem. 114 (1) (2013) 220–229, https://doi.org/10.1002/jcb.24357.
[50] B. Huang, M. Chen, J. Tian, Y. Zhang, Z. Dai, J. Li, W. Zhang, Oxygen-carrying and antibacterial fluorinated nano-hydroxyapatite incorporated hydrogels for enhanced bone regeneration, Adv. Healthc. Mater. 11 (12) (2022), e2102540, https://doi.org/10.1002/adhm.202102540.
[51] Y. Huang, C. Wu, X. Zhang, J. Chang, K. Dai, Regulation of immune response by bioactive ions released from silicate bioceramics for bone regeneration, Acta Biomater. 66 (2018) 81–92, https://doi.org/10.1016/j.actbio.2017.08.044.
[52] K.J. Oldknow, V.E. MacRae, C. Farquharson, Endocrine role of bone: recent and emerging perspectives beyond osteocalcin, J. Endocrinol. 225 (1) (2015) R1–R19, https://doi.org/10.1530/JOE-14-0584.
[53] C. Ge, Q. Yang, G. Zhao, H. Yu, K.L. Kirkwood, R.T. Franceschi, Interactions between extracellular signal-regulated kinase 1/2 and P38 MAP kinase pathways in the control of RUNX2 phosphorylation and transcriptional activity, J. Bone Miner. Res. 36 (10) (2021) 2096–2097, https://doi.org/10.1002/jbmr.4300.
[54] H. Gu, F. Guo, X. Zhou, L. Gong, Y. Zhang, W. Zhai, L. Chen, L. Cen, S. Yin, J. Chang, L. Cui, The stimulation of osteogenic differentiation of human adipose-derived stem cells by ionic products from akermanite dissolution via activation of the ERK pathway, Biomaterials 32 (29) (2011) 7023–7033, https://doi.org/10.1016/j.biomaterials.2011.06.003.
[55] L. Li, X. Chu, Y. Yao, J. Cao, Q. Li, H. Ma, (-)-Hydroxycitric acid alleviates oleic acid-induced steatosis, oxidative stress, and inflammation in primary chicken hepatocytes by regulating AMP-activated protein kinase-mediated reactive oxygen species levels, J. Agric. Food Chem. 68 (40) (2020) 11229–11241, https://doi.org/10.1021/acs.jafc.0c04648.
[56] X. Shen, Y. Yu, P. Ma, Z. Luo, Y. Hu, M. Li, Y. He, Y. Zhang, Z. Peng, G. Song, K. Cai, Titania nanotubes promote osteogenesis via mediating crosstalk between macrophages and MSCs under oxidative stress, Colloid Surf. B-Biointerfaces 180 (2019) 39–48, https://doi.org/10.1016/j.colsurfb.2019.04.033.
[57] X. Li, J. Shi, X. Dong, L. Zhang, H. Zeng, A mesoporous bioactive glass/polycaprolactone composite scaffold and its bioactivity behavior, J. Biomed. Mater. Res., Part A 84 (1) (2008) 84–91, https://doi.org/10.1002/jbm.a.31371.